CZECH TECHNICAL UNIVERSITY IN PRAGUE
Faculty of Mechanical Engineering
Department of Automotive, Combustion Engine and Railway Engineering

Sample handling and proportional dilution for cell exhaust exposure in a toxicological incubator

2019

Submitted by: Rajesh Rameswaran
Supervisor: doc. Michal Vojtíšek, Ph.D.

Declaration of authorship

I hereby declare that this master's thesis has been written by me in person. All information derived from other works has been acknowledged in the text and the list of references.

In Prague: 19. 08. 2019

_____

Rajesh Rameswaran

Anotace

Tento experiment je založen na experimentu toxicity výfukových plynů a vyhodnocuje dlouhodobé účinky výfukových plynů zážehového motoru na tkáně lidských buněk plic. Cílem práce je navrhnout a vyvinout experimentální nastavení, které se použije pro tento experiment, a analyzovat dva typy systémů ředění výfukových plynů - systém ředění na principu rotačních disků (MD-19, Matter engineering) a gravimetrický systém ředění (Smart sampler, AVL). Analýza je založena na faktorech, jako jsou poměry ředění, koncentrace částic v čase a distribuce průměrných velikostí. Rovněž se zkoumají ztráty částic v odběrném potrubí výfukových plynů.

Klíčová slova: Částice, koncentrace částic, toxicita výfukových plynů, systémy ředění výfukových plynů, ztráty částic

Abstract

This master thesis is based on an exhaust toxicity experiment performed to evaluate the long-term effects of a contemporary spark-ignition engine exhaust on human lung cell tissues. The goal of the thesis is to design and develop the experimental setup that is used for this experiment and to analyse two types of exhaust dilution systems – a rotating disc dilution system (MD-19, Matter engineering) and a gravimetric dilution system (Smart sampler, AVL). The analysis is based on factors like dilution ratios, particle concentrations over time and mean size distributions. The losses in particulate matter through the exhaust sampling train are also investigated.

Keywords: Particulate matter, particle concentration, exhaust toxicity, exhaust dilution systems, particle losses

Acknowledgements

I would like to begin with thanking my parents for providing me with this opportunity, and for their constant support throughout the course of my education. I would also like to thank Mr. Radhakrishnan for his financial support to pursue my master's degree at this University. I would like to thank doc. Michal Vojtíšek, Ph.D., Faculty of Mechanical Engineering, Czech Technical University in Prague for giving me the opportunity to work under him, and also for his excellent supervision and guidance throughout the project. I would like to thank my colleagues from the laboratory at the Centre of Vehicles for Sustainable mobility, Roztoky for their constant support throughout the phases of experimentation. I would also like to thank Mr. Kalpita Kumar Praharaj, my fellow classmate who also worked on the same project, for his contribution and support. Finally, I would like to thank all my friends who have supported me and have been a part of my educational journey at this university. I would also like to mention the Czech Science Foundation, which supported the project under the grant no. 18-04719S: Mechanisms of toxicity of gasoline engine emissions in 3D tissue cultures and a model bronchial epithelial cell line.

Contents

1 Introduction 7
1.1 Particulate matter in SI engines 8
1.2 Legislations and environmental impact of exhaust emissions 11
1.2.1 Air quality standards of particulate matter 11
1.2.2 Health and environmental impacts of particulate matter 13
1.3 Exhaust toxicity studies 14
1.4 Design criteria for air-liquid interface system 15
2 Goal of the thesis 16
3 Experimental test conditions 17
3.1 Particle deposition conditions 17
3.2 Engine test conditions 17
3.3 Preferred exhaust sampling conditions 19
4 Experimental setup and design 20
4.1 Components used in the experiment 21
4.1.1 Dilution systems 22
4.1.2 Exposure chamber 24
4.1.3 Membrane humidifiers 25
4.1.4 Exposure boxes 26
4.1.5 Humidity and temperature monitoring systems 27
4.1.6 Flow control components 29
4.1.7 Engine Exhaust Particle Sizer 29
4.1.8 Condensation particle counter 31
4.2 Experimental design 32
4.2.1 Flow rates 32
4.2.2 Positioning of particle measurement instruments 34
4.3 Calculation procedure 35

5 Results 37
5.1 Limitations and challenges encountered during the experiment 37
5.1.1 Challenges encountered during the experiment 37
5.1.2 Flow limitations with respect to humidity and temperature 38
5.2 Verification of the humidity and temperature sensor 40
5.3 Dilution system effects 41
5.3.1 The nucleation hypothesis 42
5.4 Particle losses through the membrane humidifiers 44
5.4.1 Particle losses with the new membrane humidifier 47
5.4.2 Particle losses with the new fuel 49
6 Discussion and future scope 50
6.1 The dilution systems 50
6.2 The connection between losses and artefacts 51
6.3 Future scope 52
7 Conclusion 55
References 58
List of figures 61
List of tables 62
Appendix 63
A. Technical data of Engine Exhaust Particle Sizer 63
B. Technical data of Condensation Particle Counter 64
C. Specifications of Arduino Mega 2560 REV3 67
D. Arduino program 68

1 Introduction

One of the largest environmental risk factors today is fine particle air pollution. A considerably large number of deaths can be attributed to it, much more than the various behavioural risk factors like consumption of alcohol, smoking, physical inactivity, etc. (Health Effect Institute, State of Global Air, 2018). Just in Europe, 428,000 premature deaths were attributed to exposure to particulate matter (EEA, Air quality in Europe, 2018). This is a very important issue today, as the world is moving towards a future with clean and sustainable mobility, and particle air pollution is one of the major drawbacks of contemporary internal combustion engines.

Road transport emissions are very critical to human health as the emissions occur at close proximity to people during their everyday lives, especially in big cities. Road transportation is the largest contributor to NO_x emissions in 2016 in the EU, attributing to 39% of all NO_x emissions (EEA, Air quality in Europe, 2018). 29% of black carbon emissions, 10% of all PM_{10} emissions and 11% of all $PM_{2.5}$ emissions in 2016 in the EU are directly from road transportation (EEA, Air quality in Europe, 2018). The PM concentration levels from the same study were also over the daily limit in various parts of Europe (EEA, Air quality in Europe, 2018).

Over the years, engine exhaust emissions were reduced considerably due to new governmental regulations. However, this does not solve the problem completely as the number of vehicles on the road keeps increasing every year. There were approximately 308.3 million vehicles on European roads in 2018 (European Automobile Manufacturers Association, 2018). Though there is a rise in the electric vehicle market, with 2% of new cars that were registered in 2018 in the EU being Electric vehicles, half of the EU member states have an EV market share of less than 1%. Between the large number of combustion engine-powered vehicles on-road, and discrepancies with the on-road emissions and the legal limits, exhaust emissions still pose a problem today. Another major concern is that of the very small particles, on the order of 10nm and lower, which have the capacity to deposit in the human lung alveoli through diffusion, the capability to penetrate into the bloodstream and also into the brain via the olfactory nerve (Elder, et.al, 2006)(Oberdeorster, et.al, 2004)

1.1 Particulate matter in SI engines

Particulate matter is defined as any dispersed matter, solid or liquid, in which the individual aggregates are larger than single molecules but smaller than 500 µm (Springer, 1973). These particulates can be classified based on their size into coarse and fine particles. The fine particles are composed mainly of combustion particles, secondary aerosols that are formed in the environment and condensed vapours of organic and metal compounds (Suresh, 2018). Two metrics are defined, PM_{10} and $PM_{2.5}$, which are inhalable particles with diameters 10 µm and smaller, and 2.5 µm and smaller, respectively. PM 2.5 is a subset of PM10, and nanoparticles are defined as particles smaller than 50nm and ultrafine particles are defined as particles smaller than 100nm respectively, as shown in figure 1.1. As mentioned before, the very small particles pose a very big threat to health due to their increasing concentrations in urban areas and also the way they penetrate the human body.

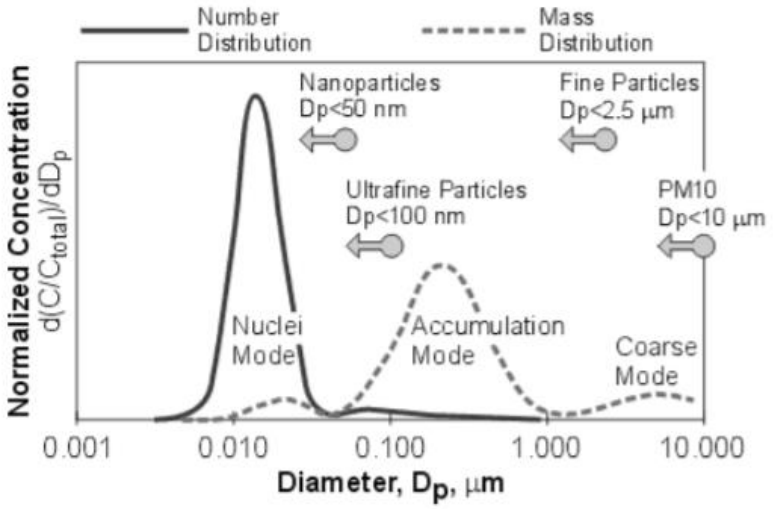

Figure 1.1 Size distribution of particulate matter (Majewski, 2016)

This thesis work is part of a project that directly deals with particulate matter exhaust from contemporary spark-ignition engines. In the UK, the number of gasoline-powered vehicles has reduced considerably over the years. But even after the reduction, around 59% of all on-road vehicles were gasoline-powered (Hull, 2018). With the governments trying to reduce the number of on-road diesel-powered vehicles, the number of gasoline-powered vehicles will only increase, as EVs are not yet mainstream, especially in the developing countries.

Spark ignition engine particulates are composed of various organic and inorganic substances. While larger particles settle down in seconds, smaller particles may be in the atmosphere for a long period of time, around several months. A combination of mechanisms occur that result in the formation of PM in SI engines: pyrolysis of fuel and lubricating oil, nucleation, and oxidation. Factors such as temperature, availability of the particle precursors like liquid fuel droplets, fuel-rich regions, and products of incomplete fuel oxidation affect particle nucleation. Combustion chamber temperature and oxygen availability affect oxidation. The amount of hydrocarbons available for absorption/adsorption and the available surface area onto which they can adhere and the number of particles with which each particle can coagulate affect particle growth (Kayes, et.al, 1999).

With respect to equivalence ratio, the size of particles has been reported to be high in the lean and rich mixtures, as temperature and availability of soot precursors plays a major role in their formation and growth. Figure 1.2 shows the number weighted particle size with respect to the equivalent ratio. It is seen here that the mean size of particles is low for the equivalence ratios close to the stoichiometric ratio where the gasoline engines are operated in.

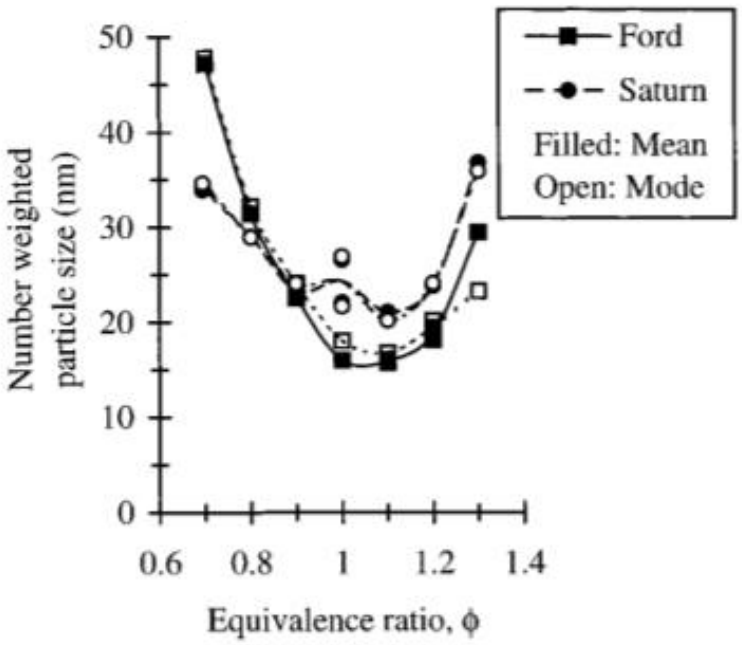

Figure 1.2 Number-weighted mean and mode particle sizes vs. equivalence ratio for two vehicles (Kayes, et.al, 1999)

Formation of particles also occurs in heterogeneous phase reactions, from liquid fuel droplets burning in air. This process depends mainly on the presence of unburnt liquid fuel droplets post-combustion, and sufficient oxygen and temperature. Thus, PM formed by this mechanism was observed at a leaner mixture, with an equivalence ratio of 0.7, in a study using optical techniques conducted by Witze and Green (1997) (Kayes, et.al, 1999).

Particle oxidation is dependent on temperature and oxygen availability. The temperature of combustion increases with a higher equivalence ratio, but the available oxygen also decreases simultaneously. Thus, the oxidized PM fraction is maximum at the lowest equivalence ratio and decreases as it is increased (Kayes, et.al, 1999).

The availability of hydrocarbons and PM surface area influence particle growth via adsorption/absorption. Low temperatures and high concentrations of both unburnt hydrocarbons and large particle surface area contribute to the formation of particles (Kayes, et.al, 1999).

Direct injection technology allows the modern SI engines to operate in leaner air/fuel ratios and also tend to have a heterogeneous charge, as opposed to older SI engines which ran very close to stoichiometric air/fuel ratios and with homogenous port fuel injection. The usability of leaner air/fuel ratios is however limited by NOx emissions due to the efficiency of the three-way catalytic converter. Heterogeneous injection facilitates the formation of PM, and hence, GDI engines produce up to twice the number of particles when compared to conventional port fuel injection engines (Mohsin, et.al, 2018). These engines also produce more ultrafine particles that are lesser than 100 nm when compared to diesel engines, and these have an adverse impact on human health (Mohsin, et.al, 2018).

According to the Euro 6 regulations, all Gasoline Direct Injection engine powered light vehicles have a PM limit of 0.0045 g/km and a Particle Number limit of $6*10^{11}$ particles/km (DieselNet, Emission Standards, 2019).

1.2 Legislations and environmental impact of exhaust emissions

As mentioned before, exhaust emissions have a big impact on humans and the environment. It is thus controlled extensively with government regulations by all the countries in the world. Different parts of the world are at different stages of emission control, with the more developed countries having stricter norms. Developing countries like India are also developing new regulations (BS-VI) to reduce the environmental impact of road vehicles. The emission limits are for commonly regulated pollutants by the Bharat Stage VI are in fact numerically equal to Euro 6 standards for similar engine types (International Council on Clean Transportation, 2016). In this section, the regulations and the situation for particulate matter in the EU are discussed.

1.2.1 Air quality standards of particulate matter

Air pollution has a direct negative impact on the quality of water, soil, and thus affects flora and fauna, in addition to human health (EEA, Air quality in Europe, 2018). Hence, for the EU, the Ambient Air Quality directives set limit values for different pollutants. Table 1.1 has information about the PM_{10} and $PM_{2.5}$ limit values.

Table 1.1 Air quality standards for the protection of health for PM, given in the EU Ambient Air Quality Directives (EEA, Air quality in Europe, 2018)

Pollutant	Averaging Period	Legal nature and concentration	Comments
PM_{10}	1 day Calendar year	Limit value:50 µg/m^3 Limit value: 40 µg/m^3	Not to be exceeded more than 35 days per year
$PM_{2.5}$	Calendar year	Limit value: 25 µg/m^3	

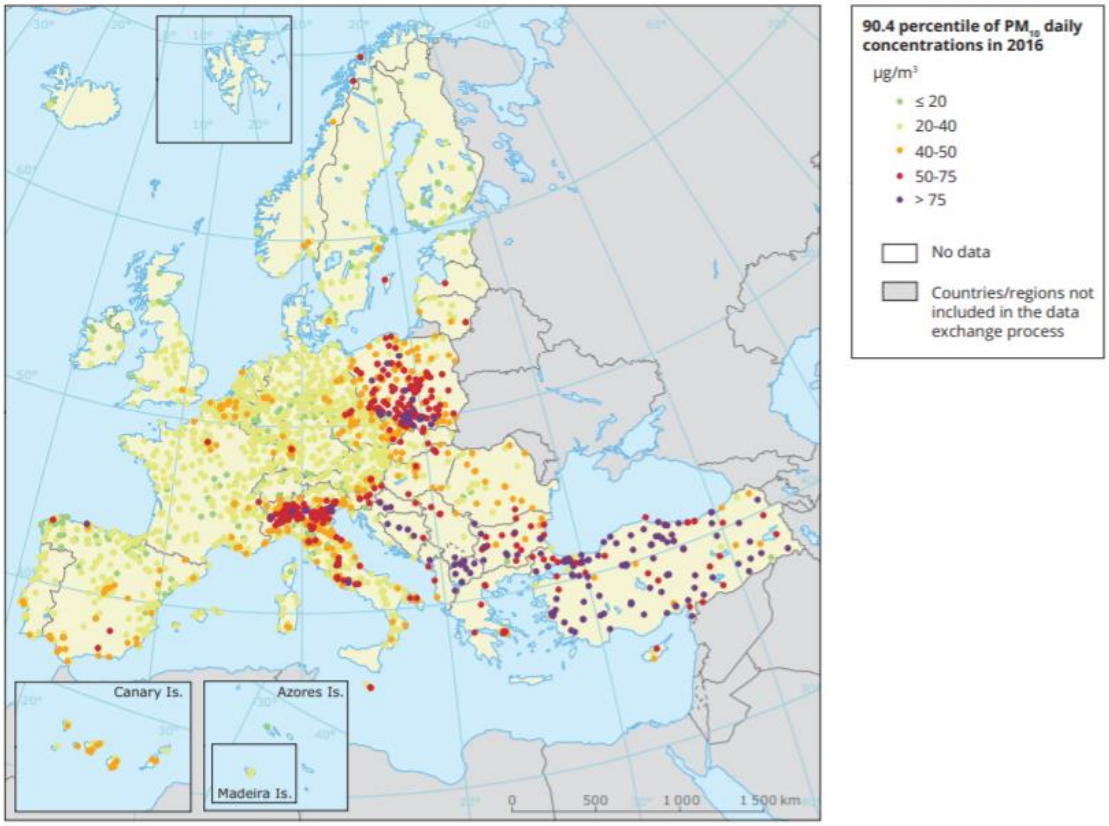

Figure 1.3 PM_{10} concentrations in 2016 with respect to daily limit value (EEA, Air quality in Europe, 2018a)

The PM_{10} concentrations at different places with respect to the limit values in 2016 are shown in figure 1.3. It can be seen that the rural concentration levels vary across the continent. Nine stations in Italy, three in Czechia, two in Turkey, and one in Slovenia exceeded the daily limit values. One rural background in Turkey also exceeded the annual limit value (EEA, Air quality in Europe, 2018). There were also isolated incidents, which were named 'pollution episodes' that happened in different quarters of the year, where different conditions led to very high concentrations of PM emissions across Europe. Hence, there is great importance in studying the effects of these particulate emissions, as the legislation alone can still not solve the issue, at least considering the current state of affairs.

1.2.2 Health and environmental impacts of particulate matter

The smaller the particles are, the greater the problems caused by them. Particles that are lesser than 10 μm in diameter, that enter the lungs and bloodstream, can cause a lot of damage to health, some of which are (United States Environmental Protection Agency, 2018):

- Premature death in people with heart or lung disease
- Non-fatal heart attacks, irregular heartbeat
- Aggravated asthma
- Increased respiratory symptoms such as coughing, difficulty in breathing, etc.

Environmental effects of air pollution include (United States Environmental Protection Agency, 2018):

- Making water bodies acidic
- Changing the nutrient balance in coastal waters and large river basins
- Depleting soil nutrients
- Damaging forests and farm crops
- Affecting ecosystems
- Contributing to acid rain

All these topics further strengthen the need to effectively study and check the levels of the different constituents of air pollution including particulate matter more precisely and study their effects better, and thus reduce them as much as possible from everyday air.

1.3 Exhaust toxicity studies

Exhaust toxicity studies were first conducted in 1986 (Barter, 1997). These were animal toxicology studies. They were performed in order to examine the health effects of gasoline and diesel exhausts by studying the systemic and pulmonary toxicity and carcinogenicity in rats and hamsters.

Since then, automotive engines have changed considerably, with repercussions in the exhaust composition. Performing epidemiological studies in exposed human populations are one of the most widely used methods for estimating the toxicity/carcinogenicity of a given compound (Vojtisek, et.al, 2019). This approach is, however, time-consuming and requires a sufficient population size to be exposed in order to obtain results. It cannot be used to assess the effects of new technology or fuel before it is considered for mass utilization. In these situations, using models of tissues to study the toxicity effects are the most viable method (Vojtisek, et.al, 2019).

There are various methods to perform these tests. Suitable compounds from particulate matter that is collected on a filter from exhaust gas can be extracted by using a suitable sorbent and be added to a solution that is fed to biological material like isolated DNA, cells, cell cultures and animal tissue slices (Vojtisek, et.al, 2019). Particles can also be used directly from the exhaust to expose the biological material.

In vitro testing methods refer to techniques of performing a procedure in a controlled environment outside of a living organism, whereas in vivo testing refers to experimentation using a whole living organism. For exhaust toxicity studies, it is ethically better to perform in vitro tests as opposed to in vivo tests that use live animals. In vitro tests using cell models with extractable organic matter (EOM) and supplied with whole vehicle exhaust are suggested to be most representative towards real-life effects of engine exhaust exposure. This method, however, needs a complex exposure system as the cell models have to be present in the engine test cell during the test.

In this project, an in vitro testing method using lung cell models is designed and employed with an exposure chamber along with supporting systems that help maintain suitable conditions for the cells. The major goal of the experiment is to evaluate different cell cultures and models, different toxicity assays, and exposure conditions, and to develop a compact exposure system that is capable of operation in an engine or vehicle testing laboratory or even on road.

1.4 Design criteria for air-liquid interface system

Vehicular exhaust is a combination of various gaseous pollutants and a complex mixture of volatile and non-volatile chemical compounds that constitute particulate matter. It is thus not optimal to perform toxicological tests with standard submerged cell cultures on such a complex mixture of chemicals (Vojtisek, et.al, 2019). Air-liquid interface systems are a physiologically relevant alternative to standard in vitro tests (Lacroix, et.al, 2018) (Geiser, et.al, 2007).

Air-liquid interfaces usually consist of cell model inserts that are placed in standardized plates of different sizes (Vojtisek, et.al, 2019). In this project, a commercially available 24-well format Transwell® cell culture inserts are used. These inserts provide a system that makes it relatively easy for transportation and also have a sufficient number of cells for toxicological analyses (Vojtisek, et.al, 2019). The cells are grown in these inserts with their bottom layer being in contact with the culture media and their apical layer being exposed to the exposed gases/air.

The criteria for the survival of the lung cell cultures are maintained with the help of mechanical systems such as an exposure chamber, membrane humidifiers, and a CO_2 tank. The optimum conditions to maintain are a temperature of 37°C, 5% excess CO_2 and relative humidity of at least 85%.

Before performing complete toxicological tests on the more expensive inserts, preliminary tests are performed on cheaper alternatives to ensure satisfactory operation of the mechanical systems and also to perform basic cytotoxicity tests to find the exposure threshold. These tests are based on the measurement of metabolic products in cells or culture medium (Upadhyay, et.al, 2018). The interpretation of these measurements is based on the fact that the toxic effects of the engine exhaust affect cell metabolism thereby resulting in lower/higher production of metabolites, slower cell proliferation or cell membrane damage (Vojtisek, et.al, 2019).

Over the period of the project, these tests were completed, and both the mechanical systems and the boxes holding the lung cell inserts were optimised so as to produce usable results with exposing the more expensive inserts to the engine exhaust.

In this project, two types of lung cell models are used: the human lung cell line BEAS -2 and the 3D lung tissue model MucilAir^{TM}(Epithelix Sarl, Geneva).

2 Goal of the thesis

The main goal of the thesis is to design an engine exhaust sampling system for an air-liquid interface exposure system in order to perform toxicological exposure tests on human lung cell models. The various tasks to perform in the experiment are to:

I. Design and assemble a sample conditioning system
II. Maintain and monitor the vital conditions required for the experimental procedure
III. Perform experiments on the sample conditioning system and tackle any challenges that arise during the course of the experiment
IV. Compare two different dilution systems that could be used for the exposure tests.
V. Evaluate particle losses through the sampling train and suggest means to make the system more efficient.

3 Experimental test conditions

This chapter deals with the experimental conditions used in the project with respect to particle deposition on the lung cells, the engine test cycle used to perform the tests and particle sampling.

3.1 Particle deposition conditions

The exhaust from the engine is initially conditioned using an exhaust dilution system and is then let to pass by the cell cultures. The exhaust is deposited on the lung cell cultures by diffusion, and the deposition rates are approximately 2% (Tippe, et.al, 2002). The deposition rate could be increased by factors like electrostatic charging of particles (Geiser, et.al, 2017), thermophoresis (Ihalainen, et.al, 2018), or inertial impaction (Cooney, et.al, 2011).

Since this project deals with exposing complete conditioned exhaust, unassisted deposition by diffusion is the chosen method, as the combined effects of the gaseous pollutants and particles could prove to be unrealistic because of varying deposition rates (Vojtisek, et.al, 2019). The conditions and setup used during the exposure of the BEAS - 2B models and the MucilAir^{TM} models are similar. This to avoid discrepancies and also to validate the whole experimental system before studying the more expensive MucilAir^{TM} models.

3.2 Engine test conditions

The aim of the whole project is to study the effects of engine exhaust on human lungs. The 1.4 litre R4 16 valve TSI/TFS gasoline direct injection engine from Volkswagen is used in this experiment. In order to give a reasonably accurate representation of the typical exposure of engine exhaust to a person in a city, the following conditions are considered:

I. A transient engine cycle, representative of typical city driving
II. Dynamic operation under load and cold start effects should be represented
III. Advanced after-treatment technology used in production engines must be present

The World Harmonized Light Vehicle Test Cycle (WLTC) is chosen as it fulfils the requirements and is also used in modern type approval tests.

The WLTC test cycles are chassis dynamometer tests developed by the UN ECE GRPE (Working Party on Pollution and Energy) group for the determination of emissions and fuel consumption from light-duty vehicles (Dieselnet, 2019). The World Harmonised Light Vehicle Test Procedure (WLTP) consisting of a set of WLTC test cycles that are different for different vehicle classes depending on their power to weight ratio, is replacing the New European Driving Cycle (NEDC) as the standard type approval procedure over 2017-2019 (Dieselnet, 2019).

WLTC test cycles are divided into three classes, class 3 for vehicles in Europe and Japan, class 2 for vehicles in India and low power vehicles in Europe and Japan, class 1 for vehicles in India (Dieselnet, 2019). Class 3 tests are for vehicles with the highest power to weight ratios and Class 1 tests are for vehicles with the lowest power to weight ratios. A typical WLTC test cycle lasts 1800 seconds, with four phases: Low, Medium, High and Extra High, as shown in Figure 3.1.

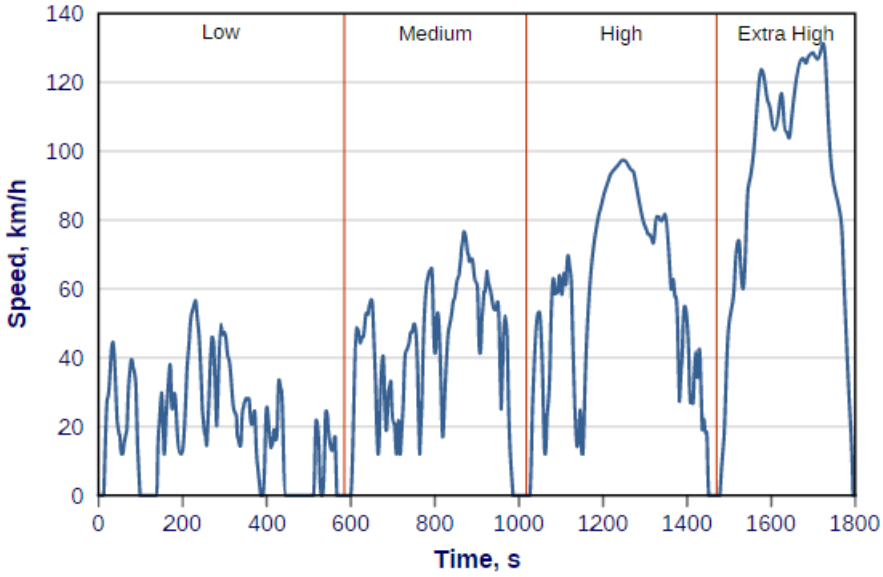

Figure 3.1 WLTC cycle for Class 3b vehicles (Dieselnet, 2019)

The WLTC thus covers the need to have a representative transient cycle, with operation under load. The experiments in this project were initially planned to have one cold start cycle in the morning, followed by three warm cycles, after which the engine was allowed to cool down, before repeating the same cycles again. The cooling time of the engine was around two hours in order to simulate cold start conditions on the same day. This method, however, proved to be too damaging for the lung cell models. As a result, the tests were reduced to two cycles per session.

3.3 Preferred exhaust sampling conditions

Exhaust conditioning and sampling is another important factor to consider when designing the experiment. Exhaust dilution is typically used to simulate the formation of particles as they would occur when the exhaust is emitted to the atmosphere (Kooter, et.al, 2013). In this case, since a transient engine cycle is chosen, the flow of the exhaust gases varies throughout the cycle. This exhaust flow will be about dozens of times higher during maximum speed and load as opposed to idle conditions for a typical gasoline engine (Vojtisek, et.al, 2019).

To keep the volume of sampled exhaust proportional to the total exhaust flow, a full flow dilution system with a constant volume sampler (CVS), or some partial flow dilution system is typically used. The exhaust is diluted by a variable amount in order to maintain a constant flow of the diluted exhaust in order to simplify exhaust analysis.

There are however some issues associated with this method for toxicity assays. A large portion of the toxic effect of engine exhaust has been associated with its semi-volatile fraction, and these have an issue with deposition and re-entrainment in the dilution tunnels (Vojtisek, et.al, 2019). Hence, a constant dilution ratio of 10:1 is typically used in most studies.

The exhaust flow varies over the duration of the test cycle, but since the exposure occurs at a very low flow rate, there will not be a problem of particle deposition irrespective of the phase of the cycle. The partial dilution systems used in the experiment, which will be discussed later in the report, also produce very comparable results to a full flow dilution tunnel, even at relatively low particle concentrations (Pham, et.al, 2018).

Also, it is more realistic to have a constant dilution ratio as it is more representative of the way the exhaust mixes with ambient air. For this experiment, a constant dilution ratio of 10:1 is chosen, as is typically used in most toxicological studies.

4 Experimental setup and design

The basic design of the effective sampling system used for this experiment is shown in figure 4.1. It can be seen that there are two sets of exposure boxes containing lung cell culture samples. Two boxes are exposed with engine exhaust, which will have the exposed samples. The other two boxes are exposed with filtered air, which will have the control samples. Membrane humidifiers are used to achieve a high relative humidity that is required for the survivability of the lung cell cultures. This whole system is placed inside a toxicological incubator that maintains the setup at 37°C. Exhaust dilution is achieved with the help of a proportional gravimetric dilution system. A CO_2 tank is used to provide a 5% excess of the gas to both samples, as is present in the human lungs. Flow control is achieved with the help of a vacuum pump and rotameters. These components are discussed in detail in the next section.

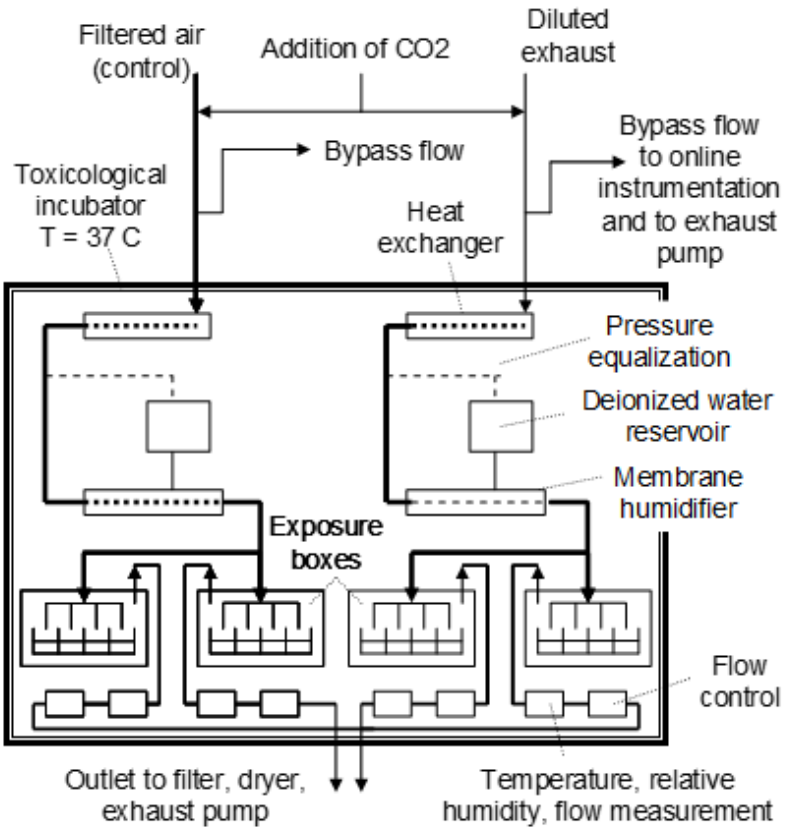

Figure 4.1 Exposure system sampling train (Vojtisek, et.al, 2019)

4.1 Components used in the experiment

The major components used in this experiment, as seen in figure 4.2, are:

I. Two dilution systems – A proportional gravimetric dilution system from AVL called the SmartSampler, and a rotating disc diluter from Matter Engineering called the MD-19.
II. A CO_2 tank
III. An exposure chamber
IV. Membrane humidifiers
V. Exposure boxes
VI. A vacuum pump
VII. Rotameters
VIII. Humidity and temperature monitoring systems
IX. An Engine Exhaust Particle Sizer (EEPS) from TSI
X. A Condensation Particle Counter (CPC) from TSI

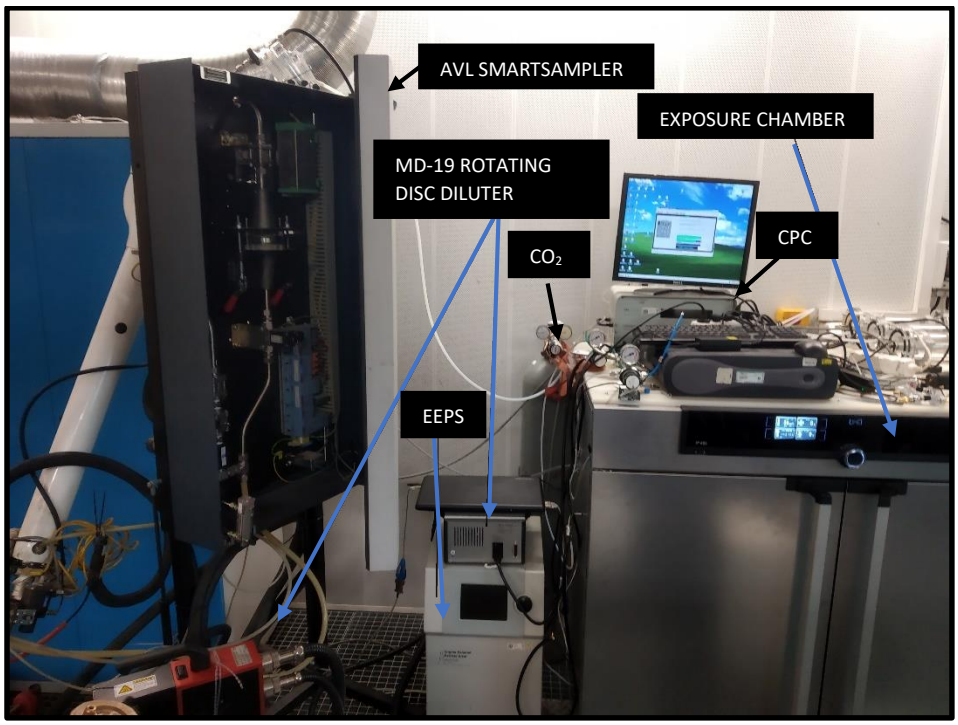

Figure 4.2 Experimental setup

They are discussed in detail in this section.

4.1.1 Dilution systems

The first major component used in the experiment would be the dilution system that is used to condition the exhaust from the engine before exposing it on the lung cell models. For this project, a proportional gravimetric dilution system from AVL called the SmartSampler is chosen. A viable alternative to this system, a rotating disc diluter from Matter Engineering called the MD-19 is also explored in parallel.

4.1.1.1 AVL SmartSampler

The AVL SmartSampler is a partial flow proportional gravimetric dilution system (see figure 4.3). This type of dilution system maintains a constant flow of the diluted sample through the gravimetric filter and regulates the inflow of the exhaust indirectly by varying the flow of filtered air (Vojtisek, et.al, 2019).

Figure 4.3 AVL SmartSampler

For the purpose of this experiment, a bypass path is created before the engine exhaust flows to the filter, at the upstream junction, in order to extract the sample flow, as shown in figure 4.4. An equivalent flow of filtered air is supplied back to the dilution system at the downstream junction to make it a closed system.

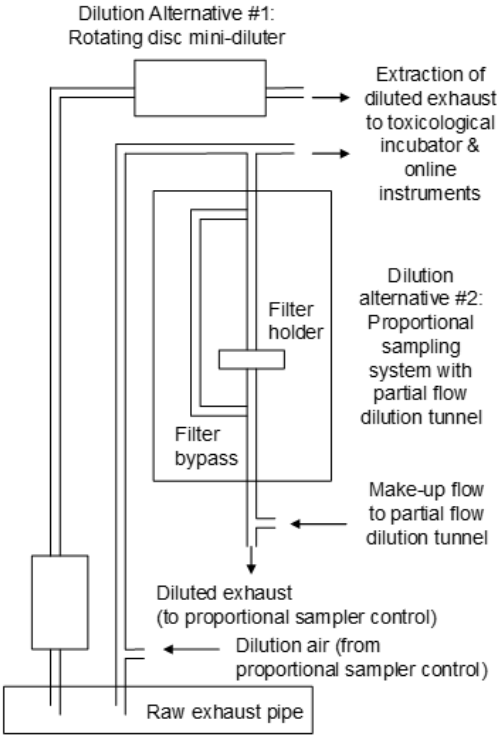

Figure 4.4 Exhaust dilution system (Vojtisek, et.al, 2019)

4.1.1.2 Matter Engineering MD-19

The MD-19 is a rotating disc dilution system from Matter Engineering (see figure 4.5). This type of dilution system consists of a rotating disc which transfers a metered quantity of sample from the sample inlet into the stream of dilution air (Homolya, et.al, 1972).

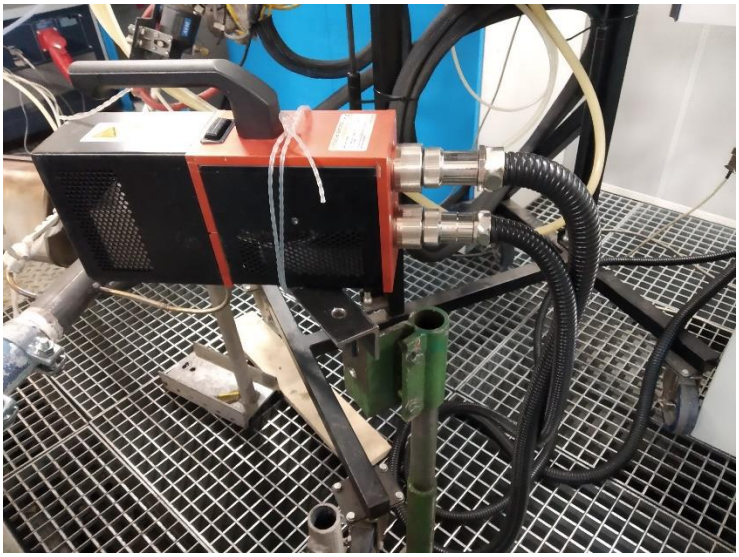

Figure 4.5 MD-19 Rotating disc diluter

The dilution ratio is controlled by varying the speed of the disc's rotation, i.e. the faster the rotation the lesser the dilution ratio. In this experiment, this system is studied as an alternative to the proportional dilution system and is connected in parallel to the other system, as shown in figure 4.2.

4.1.2 Exposure chamber

A toxicological incubator is used as the exposure chamber, inside which the lung cell cultures are placed, as shown in figure 4.1. The function of this chamber is to maintain the temperature of the whole system at 37°C. The membrane humidifiers and the exposure boxes containing the lung cell cultures are placed inside this chamber, as shown in figure 4.6. The black conductive pipes are used for the exposed samples, in order to reduce particle losses during transmission, and the white flexible pipes are used for the control samples.

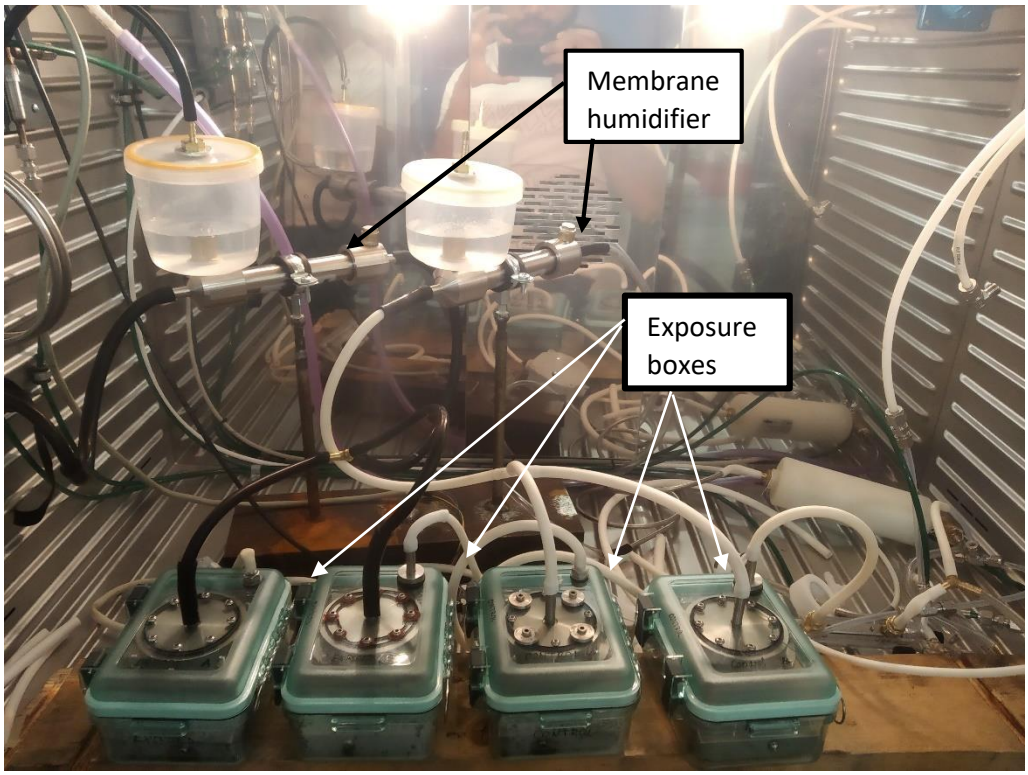

Figure 4.6 The inside of the exposure chamber

4.1.3 Membrane humidifiers

As discussed before, the humidity of the whole system has to be around 90%, or at least over 85%. To achieve this, membrane dryers are used as humidifiers in this case, as shown in figure 4.6. The membrane dryers used for initial testing were of the model FC125-240-5MR from PermaPure.

This series of humidifiers are shell and tube moisture exchangers that allow the transfer of water vapour (Permapure, 2019). The water molecules are absorbed into the walls of the Nafion® tube and subsequently transferred to the dry gas stream. This occurs due to the difference in partial pressures of water vapour on the opposing sides, as shown in figure 4.7 (PermaPure, 2019).

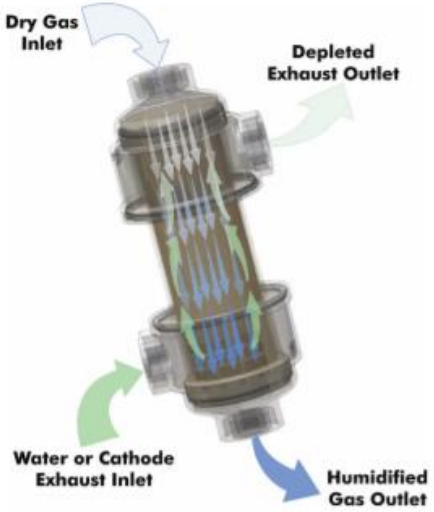

Figure 4.7 Principle of FC™ Series Humidifiers (PermaPure, 2019)

To mount these humidifiers in the experimental setup, a simple clamp was built on to a stand, and a plastic water reservoir was fixed at the water inlet, as shown in figure 4.6. The plastic reservoir holds deionized water. The effect of the difference in pressure across the membrane is reduced by pneumatically connecting the cap of the water reservoir to the sample inlet inside the exposure chamber.

These humidifiers are replaced with the PermaPure model no. MD-700-06S-1, which was specifically designed for use with aerosols. These humidifiers are shown in figure 4.6.

4.1.4 Exposure boxes

The exposure boxes that are used in this experiment were fabricated by Pechout.M and Macoun.D from the Czech University of Life Sciences in Prague. The design was based on a standard 128x86 mm 24 well plate. It houses 24 inserts with a membrane on which the lung cell cultures are deposited. A distributed head made of stainless steel, fabricated in-house, is fixed on top of the boxes in order to split the flow into eight paths with equivalent geometry, each ending with a 5mm outer diameter tube facing the membrane of the insert, as shown in figure 4.8 (Vojtisek, et.al, 2019).

Figure 4.8 Exposure box with a sample divider head showing paths for flow division (Vojtisek, et.al, 2019)

Before the fabrication of the high-cost boxes, initial flow analysis was conducted to verify the optimum distance of the lung cell inserts from the distributor head pipes, as shown in figure 4.9. The design follows the flow of air through the single entry point of the distributor head and then is channelled to two pipes instead of eight, as it is a simple 2-dimensional analysis. The requirement was to have zero velocity at the base layer, but not for a large area as that would prevent diffusion to the cells. The optimal gap was agreed to be 2.55mm by making comparisons between the CFD analysis and trial and error runs. At this chosen gap of 2.55mm, there was a small flow velocity around $1.07*10^{-1}$ m/s over the cell tissue which facilitated diffusion, while not being high enough to damage them (tested experimentally).

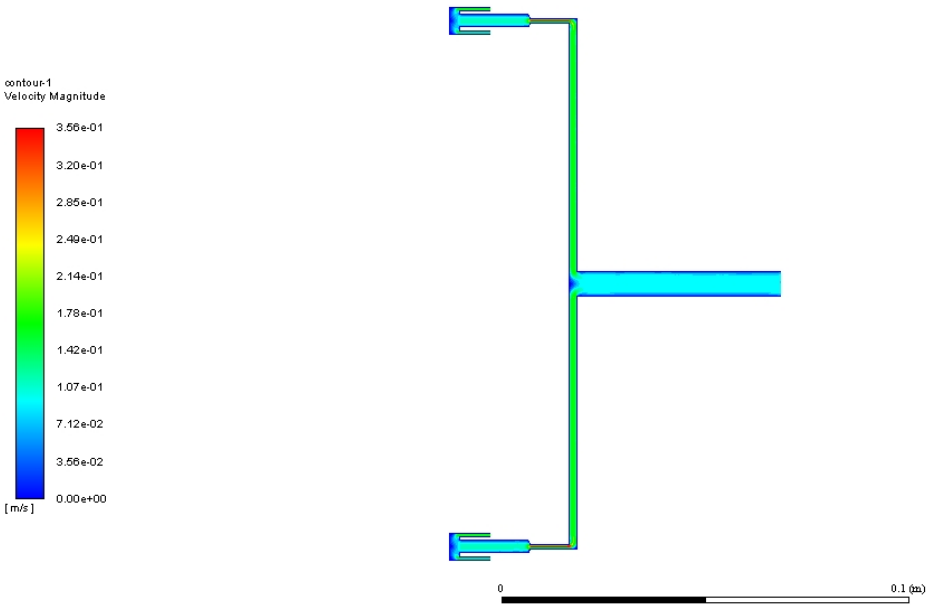

Figure 4.9 CFD Flow analysis to optimise gap between distributor head and lung cell inserts

4.1.5 Humidity and temperature monitoring systems

The importance of maintaining relative humidity and temperature is evident from the previous sections. Thus, it is essential to fabricate a system that constantly monitors these parameters. A relatively low-cost in-house system was developed. A capacitive type temperature and humidity sensor 'DHT22' (see figure 4.10) which gives a digital output was coupled with an Arduino Uno microcontroller in order to constantly monitor the relative humidity and temperature using a serial port. The basic version of the code for the Arduino program is in the appendix. This data was recorded using another open-source software named 'GoBetwino'.

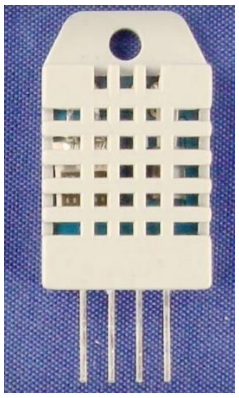

Figure 4.10 DHT22 temperature and humidity sensor (Aosong Electronics Co., Ltd, 2019)

The specifications of the DHT22 were sufficient for this application while being cost-effective at the same time. They are listed in Table 4.1.

Table 4.1 Specifications of DHT22 sensor (Aosong Electronics Co., Ltd, 2019)

Model	DHT22
Power supply	3.3-6V DC
Output signal	Digital signal via a single bus
Sensing element	Polymer capacitor
Operating range	Humidity 0-100% RH; Temperature -40 – 80°C
Accuracy	Humidity ±2% RH; Temperature <±0.5°C
Resolution	Humidity 0.1%RH; Temperature 0.1°C
Repeatability	Humidity ±1% RH; Temperature ±0.2°C
Sensing period	Average: 2 seconds

The sensor had to be housed in an air-tight system in order to effectively measure the parameters in the fluids flowing through the system. Thus, an air-tight electrical junction box was used to house the sensor. Three sides of the box were hole-punched, and the sensor was put into one side, and the inlet pipe was on one side and the outlet pipe was on the other side, as shown in figure 4.11. All three sides were sealed with the help of silicon sealant and rubber seals. The monitoring system is positioned after the exposure boxes in the circuit to measure the effective relative humidity and temperature of the fluids right after they are exposed to the lung cell models. This gives a reasonably accurate measure of conditions the lung cell cultures are subject to in real-time.

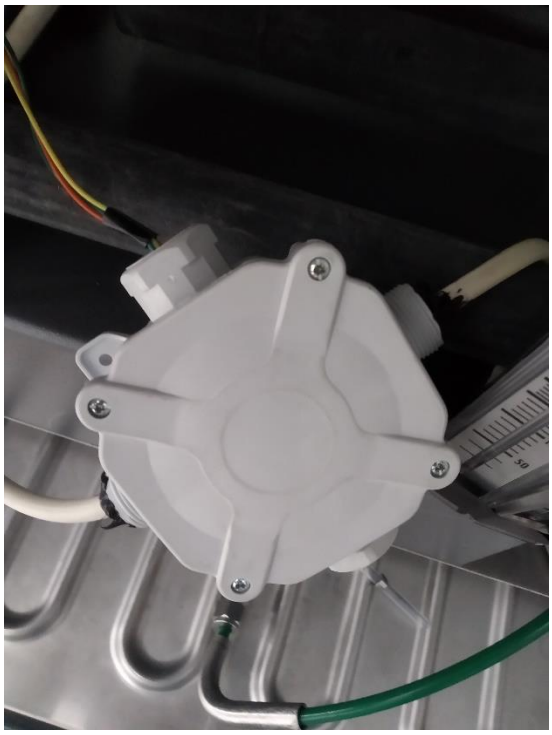

Figure 4.11 Humidity and Temperature box

4.1.6 Flow control components

A vacuum pump is used to create the flow of fluids through the whole circuit. Rotameters are used to maintain proper flow rates of CO_2, to provide return flow in the SmartSampler, to control the bypass flow back to the pump and to maintain proper flow into the exposure boxes indirectly by controlling the flow on the outlet, assuming that there are no leaks. The latter is very important as even a slightly higher flow can damage the lung cell models.

4.1.7 Engine Exhaust Particle Sizer

The Engine Exhaust Particle Sizer (EEPS) Spectrometer 3090, manufactured by TSI Incorporated, is used in this experiment to measure particle size distribution. It is a fast response, high-resolution instrument that measures particulate matter of very small sizes, from 5.6 to 560 nanometres (TSI Incorporated, 2005). With a time resolution of 10 Hz, it is well suited for dynamic testing, and in this case, the WLTC.

The EEPS works on the principle of size-based particle size segregation, as shown in figure 4.12. The instrument first draws the exhaust sample into the inlet. The flow rate into the instrument is 9.0lpm. The experiment is run with the exhaust flowing at 2.0lpm to the inlet of the exposure chamber, before the bypass line. Thus, an additional system built in-house uses a HEPA filter and a control valve to supply a controlled quantity of additional filtered air before the inlet to the EEPS, so that the exhaust gases can be supplied at a constant 2.0lpm to the EEPS, in order to replace the bypass flow that was created to improve the metering of CO_2 into the system. The exhaust reaches the exposure boxes at a flow rate of 0.2lpm, but this is very low to be accurately measured by the instrument. Hence, the next best option is the 2.0lpm at the inlet to the exposure chamber.

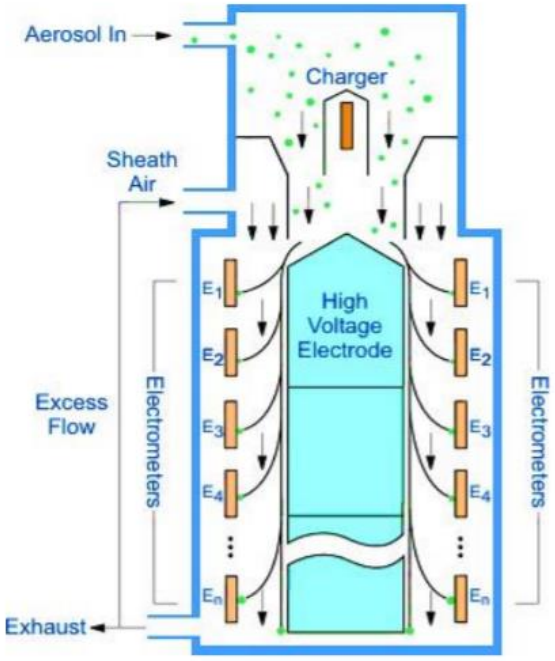

Figure 4.12 Engine Exhaust Particle Sizer flow schematic (TSI Incorporated, 2005)

The particles are then positively charged to a predictable level with the help of a corona charger. They are then transported through a high voltage electrode column with the help of HEPA filtered sheath air, where the total flow rate is 40lpm. A positive voltage is applied to the column, creating an electric field that repels the positively charged particles outwards depending on their level of charge (TSI Incorporated, 2005).

These charged particles strike electrometers that are placed around the column. The particles with higher charge strike the electrometers at the top, and the particles with subsequently lower charge strike the electrometers that are present lower down the column. The electrometers have high sensitivity, which makes it possible to measure multiple particle sizes continuously (TSI Incorporated, 2005). A built-in Digital Signal Processor (DSP) is used to synchronise time delay between the electrometers, particle charge variability, image charge and also to present a size distribution with respect to time as output (TSI Incorporated, 2005).

4.1.8 Condensation particle counter

A condensation particle counter from TSI Incorporated, CPC Model 3022, is used in this experiment to measure particle number concentrations. This instrument can detect particles with a diameter as low as 7nm. It has two modes of detection, single-count and photometric modes, which enables accurate measurements for concentrations as high as 10^7 particles/cm^3 (TSI Incorporated, 2019).

The flow rate of exhaust into the CPC is 0.3lpm, which is very ideal for the experiment, as it is very close to the exposure box flow of 0.2lpm. This is a continuous, laminar flow, thermally-diffusive instrument which uses butanol to enlarge particles through condensation, after which they are detected by optical methods (Bischof, 2006). Particles smaller than 50nm are generally undetectable by optical methods, which is why a working fluid, in this case, n-butanol is used to enlarge the particles to a size of 10-12µm through condensation (Centre for Atmospheric Science, 2019).

The process of controlled super-saturation, to typically about 100-200% is maintained in order to induce nucleation on the particles that subsequently enlarges them. The method used to achieve this is called diffusional thermal cooling, where the exhaust passes through a heated porous block or wick that is in contact with butanol and becomes saturated (Centre for Atmospheric Science, 2019), as shown in figure 4.13.

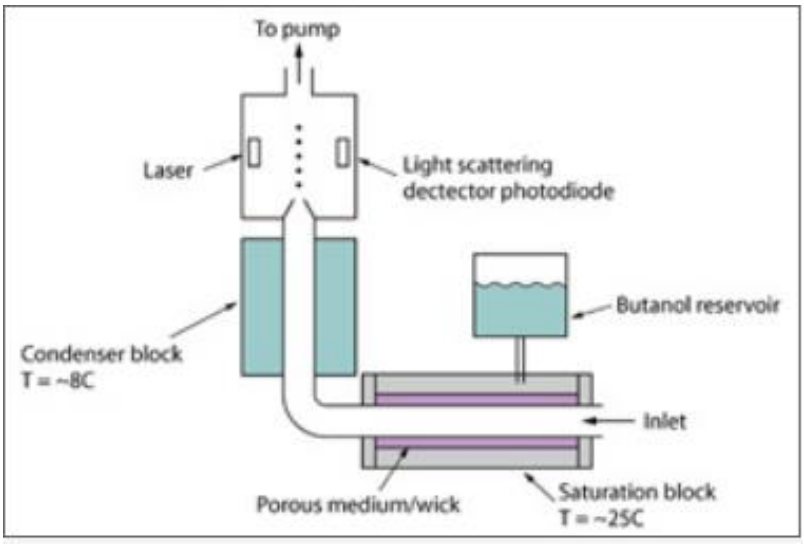

Figure 4.13 Schematic of a Condensation Particle Counter (Centre for Atmospheric Science, 2019)

The enlarged particles are then detected and counted by laser scattering, similar to standard optical particle counters. The CPC is used in this experiment as an additional instrument to measure particles at different points in the system, in conjunction with the EEPS. The particle measurements obtained from the EEPS and CPC have to be comparable to make parallel comparisons. The two instruments have been compared and found to produce similar results (Praharaj, 2019)

4.2 Experimental design

This section deals with the various conditions designed to be used in the experiment. The important factors to consider are flow rates at various points, positioning of the particle measurement instruments and dilution systems for various cases.

4.2.1 Flow rates

The flow rates at various points in the experiment are very crucial as the lung cell cultures have a strict limit in order to fulfil their survivability conditions. The major inputs to the exposure boxes housing the lung cell cultures, as discussed before, are the exhaust flow, control airflow and the excess CO_2 flow. The schematic of the flow rates in all parts of the experiment is shown in figure 4.14.

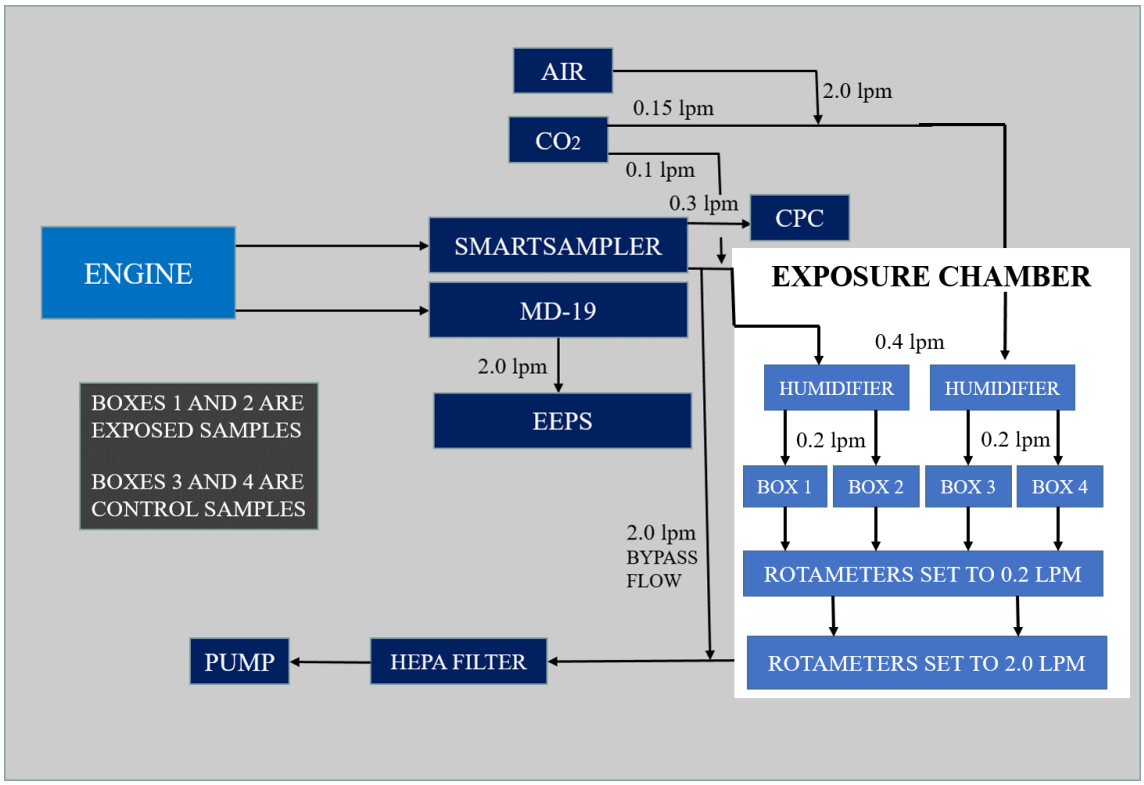

Figure 4.14 Schematic of flow rates

The flow rates at each point are discussed in detail in this section. A sample is taken from the exit of the SmartSampler that goes to the CPC at 0.3lpm for particle concentration measurement. The SmartSampler is also used as the dilution system to expose the lung cell cultures. This is because the MD-19 does not have the capability to achieve the planned low dilution ratio of 10:1. Hence, a line from the SmartSampler goes to the exposure chamber, with a bypass flow of 2.0lpm also leading back to the pump through a HEPA filter. The MD-19 is used in parallel to the SmartSampler. From the Engine, another sample is diluted, and this goes to the EEPS at a flow rate of 2.0lpm for parallel particle concentration measurement. Ambient air for the control samples is supplied through a rotameter at 2.0lpm. The 5% excess CO_2 that is required for simulating realistic conditions is supplied from a tank. The flow rate of CO_2 to the exposed samples inlet is 0.1lpm and the flow rate to the control samples inlet is 0.15lpm, each mixing with the exhaust and ambient air respectively. The value is lesser for the exposed sample, as the exhaust sample which is diluted 10:1 already contains about 1.4% CO_2.

The rest of the system is placed inside the exposure chamber. The flow through the membrane humidifiers that are used to humidify the incoming air to each set of the samples is 0.4lpm, after which the flow is split to 0.2lpm at the inlet of each exposure box. The humidity and temperature monitoring system is present after each exposure box, followed by a rotameter controlling the flow at 0.2lpm. There is another rotameter controlling a return flow of 2.0lpm from the control samples to the pump. This is thus a complete closed circuit fluid system that operates using the principle of suction by the vacuum pump.

4.2.2 Positioning of particle measurement instruments

By default, for the regular exposure tests, the CPC is used to sample particles from the SmartSampler, taking a line in parallel from the main line that goes into the exposure chamber as explained in the previous section. The EEPS is used to sample particles directly from the MD-19, with a modified inlet flow of 2.0lpm as explained in the previous section.

In order to study the particle losses through the sampling train, for these 'special cases', the following various different configurations are used:

I. CPC sampling from the SmartSampler after the humidifier at 0.3lpm, EEPS sampling from the MD-19 before the humidifier at 2.0lpm.
II. CPC sampling from the SmartSampler after the humidifier at 0.5lpm, EEPS sampling from the MD-19 before the humidifier at 2.0lpm.
III. EEPS sampling from the SmartSampler before the humidifier at 2.0lpm, CPC sampling from the MD-19 after the humidifier at 0.3lpm.
IV. EEPS sampling from the SmartSampler before the humidifier at 2.0lpm, CPC sampling from MD-19 after the humidifier at 0.5lpm.

In the first two configurations, the SmartSampler is connected to the inlet of the exposure chamber, and for the following two configurations, the MD-19 is connected to the inlet of the exposure chamber. The 0.5lpm flowrate is created across the humidifier by connecting the CPC in parallel to an exposure box, as the exposure box circuit draws a 0.2lpm flow and the CPC draws 0.3lpm flow.

4.3 Calculation procedure

The major part of the investigation performed in this thesis is the data analysis of data that was measured by the EEPS and CPC. The basic relation that is required in order to make the comparisons for this master thesis is that the EEPS and CPC provide repeatable comparable results, as explained in section 4.1.8.

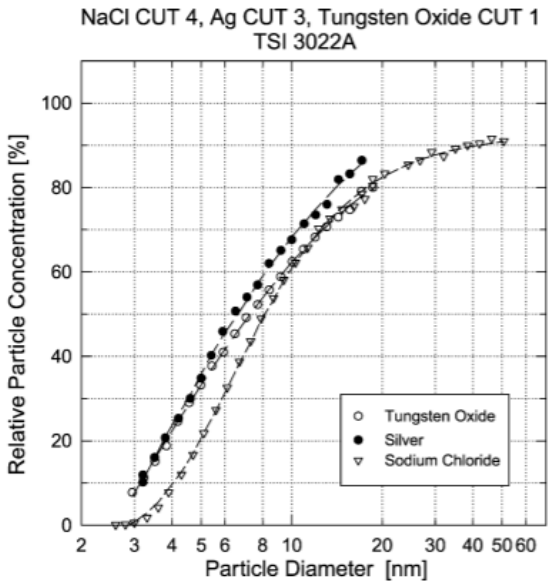

Figure 4.15 Comparison of the response characteristics of the TSI 3022A CPC with respect to NaCl, Ag and Tungsten oxide test aerosols (Ankilov, 2002)

The first step in the calculation procedure is to find the CPC equivalent particle concentration for the concentration collected from the EEPS. The CPC has a measurement efficiency that is dependent on particle size. Sintered silver particles have been recommended as a suitable calibration aerosol for soot particles (Nowak, et.al, 2014). The detection efficiency of silver particles with respect to particle size is shown in figure 4.15.

The detection efficiency increases with particle diameter. This factor is taken into consideration when the comparisons are made between particle concentrations measured by the EEPS and the CPC. Since the EEPS measures particles based on their size, it is easy to derive the particle number concentration that would theoretically be detected by the CPC from EEPS size distribution by multiplying the measured particle concentration in each size bin by the corresponding CPC detection efficiency.

Since the two dilution systems operate with different dilution ratios, the next step is to calculate the equivalent raw exhaust particle concentrations from each set of values in order to perform direct comparisons. Depending on the configurations used in the tests, there are different calculations that are followed for determining the raw exhaust concentrations for each case, as follows:

I. When CPC samples from SmartSampler – 10:1 from the SmartSampler and CPC has no additional dilution
II. When EEPS samples from SmartSampler – 10:1 from the SmartSampler and additional dilution in the EEPS of 9/2:1 = 45:1
III. When CPC samples from MD-19 – 95:1 from the MD-19 and CPC has no additional dilution
IV. When EEPS samples from MD-19 – 95:1 from the MD-19 and additional dilution in the EEPS of 9/2:1 = 425:1

The basic method of making comparisons is to identify the distinct beginning and end of each WLTC cycle. When comparing the results obtained in different runs conducted consequently or on the next day, the beginning of the cycle has to be synced for all the cycles that are being compared.

All the comparisons are shown in the logarithmic scale as this avoids skewness towards large values. Some values, especially at the beginning of the tests and during cold start are much greater than other values. There are also some values that are discrepancies due to some artefacts in the system. It is thus advantageous to use the logarithmic scale to visualise the whole cycle more clearly.

In some cases, for further analysing a set of data, mean size distributions are also plotted. This can be done only with the results obtained from the EEPS as it records size dependant particle concentration. To do this, one distinct cycle is first chosen, and the average concentration over the entire cycle for each particle size is found. Then, a graph between the particle size and average particle concentration for each size is plotted.

5 Results

There were multiple phases of experimentation over the first half of 2019, with slight variations in the system throughout the different phases. There were two sets of membrane humidifiers, two types of lung cell models, varied exposure times and slight mechanical modifications during the course of the test. The combined results of all the tests are discussed in this chapter, after first discussing the challenges encountered during their execution.

5.1 Limitations and challenges encountered during the experiment

There were limitations for the flow rates through the membrane humidifiers and various everyday challenges that were dealt with during the course of testing. These are discussed in this section.

5.1.1 Challenges encountered during the experiment

There were various challenges and problems that arose during the course of the experiment. Some of the major issues were:

I. Problems with flow rates: The rotameters were set to maintain a constant flow rate at each location. In reality, however, during initial testing, the flow was always fluctuating by a small amount, and in some locations to a considerable extent, in addition to sometimes having a different flow rate than the amount shown in the rotameter. This is not desirable as it can completely damage the lung cell models. A flow meter was used to carefully measure the 'actual' flow rate and calibrate each rotameter before installing the exposure boxes. The flow was checked and adjusted during the course of a whole test day to try and ensure as accurate of a procedure as possible.

II. Deionised water container leakage and flow rate problems: The water container for the membrane humidifiers developed leaks during initial testing and had to be repaired. There were some discrepancies with the flow rates in the system, which were found to be caused due to the container lid not being tight. This was fixed during initial testing and also constantly checked during the course of the experiment.

III. Exposure box leakage: One exposure box developed some leaks, and this was very dangerous for the lung cells as they have to be in a sterile environment, and this would also mean that the cells are not exposed properly. All the boxes were thus checked for leaks and fixed diligently.

IV. Miscellaneous issues: There were some issues caused due to the flow of compressed air to the SmartSampler, some malfunctioning of the instruments and with data collection from them that were dealt with and solved on a day to day basis.

Most of the major problems and challenges were dealt with in the initial stages of testing, and the system was perfected during the course of experimentation. This method allowed to better understand the working of the various components and instruments and to make sure the data that was collected were reliable.

5.1.2 Flow limitations with respect to humidity and temperature

One of the major goals of this thesis is to analyse and reduce particle losses. The membrane humidifier is the most important component to investigate in terms of particle losses as it has a semi-permeable membrane that is not conductive. Apart from this, conductive pipes are used up until the exposure boxes. The basic theory used in this investigation is that the particle losses are increased with a decreased flow rate. Thus, the maximum flow at which the membrane humidifier can operate without losing considerable relative humidity and temperature was studied.

Special tests were conducted without using the engine. The vacuum pump was operated to create suction, and ambient air was sent into the exposure chamber. A rotameter was used to maintain and increase the flow in steps over a period time and the effects of flow on relative humidity and temperature were studied.

The flow rates at which the tests were carried out were 0.2lpm, 0.5lpm, 1.0lpm and 2.0lpm. The optimal flow rate that was desired was 2.0lpm as that is the flow outside the exposure chamber. It would thus be beneficial to connect the membrane humidifiers at this point to reduce particle losses as explained previously. The results of the experiment are shown in figures 5.1 and 5.2.

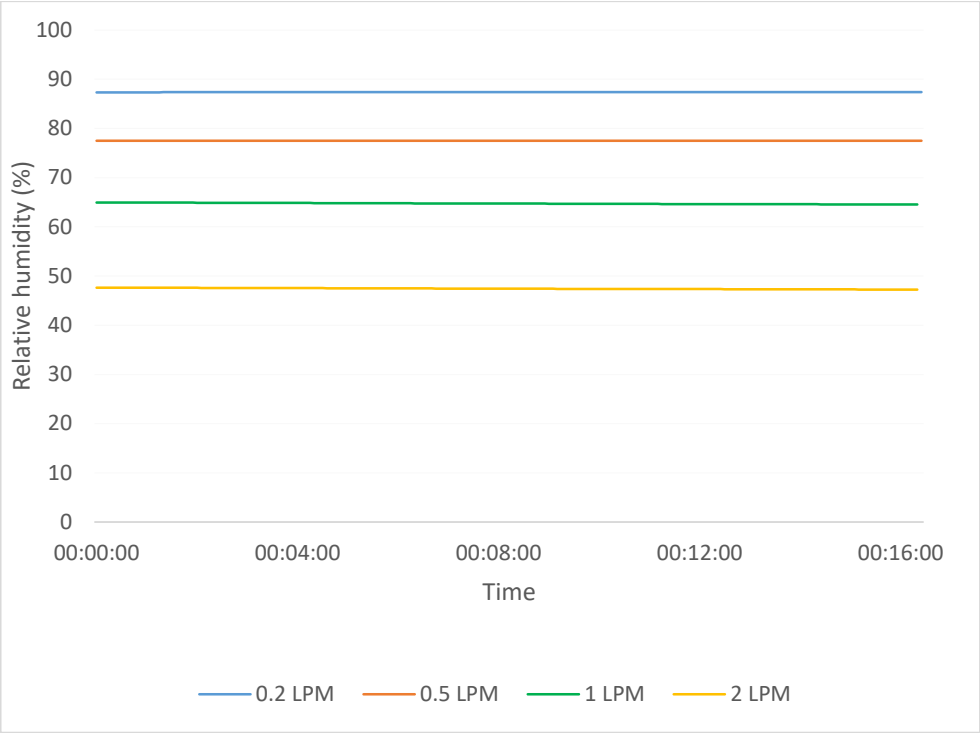

Figure 5.1 Relative humidity vs time with different flow rates

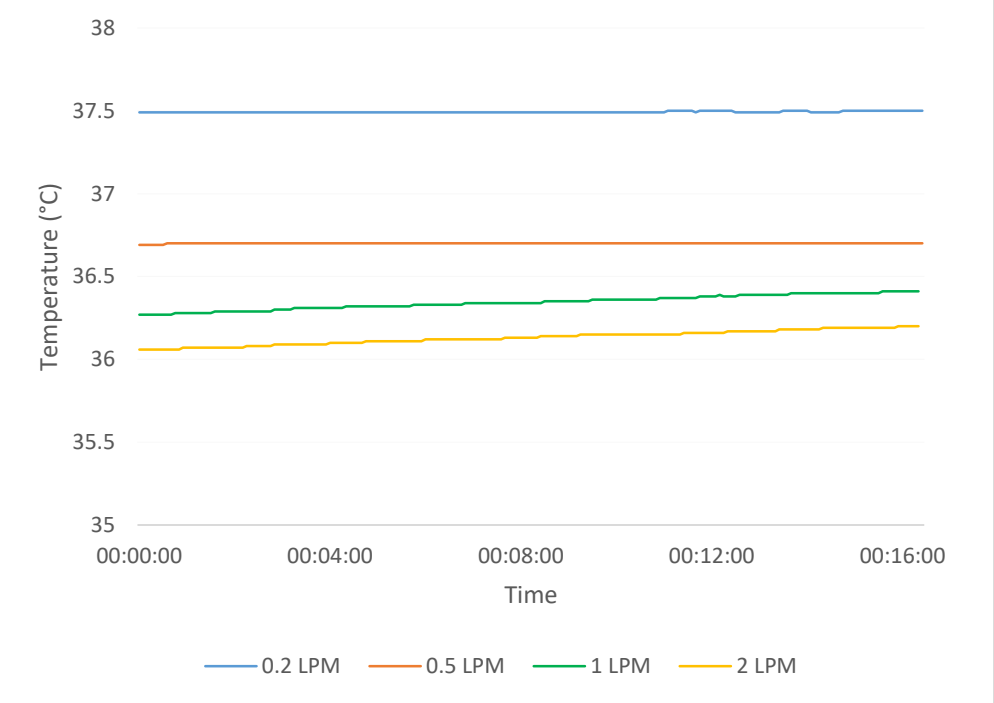

Figure 5.2 Temperature vs time for different flow rates

It can be seen that the maximum acceptable flow rate after which the increase in sample humidity is insufficient is 0.5lpm. The temperature also reduces with an increased flow rate despite the presence of a heat exchanger inside the exposure chamber.

Another possible solution could be to increase the temperature control of the exposure chamber higher than 37°C, but there is a problem of the general ambient temperature of the chamber increasing to an unbearable level for the health of the lung cell cultures. Thus, the flow is bottlenecked at 0.5lpm. The tests are thus performed at a flow rate of 0.4lpm, which is basically one membrane humidifier for two exposure boxes.

5.2 Verification of the humidity and temperature sensor

The humidity and temperature system was fabricated in-house and was also relatively low cost. Thus, a reference sensor from Vaisala, the HUMICAP® Humidity and Temperature Probe HMP113 was used to verify the functioning of the DHT22 sensor. This sensor was chosen as it has excellent stability and is an industry-grade sensor with an IP54 classification (Vaisala, 2019).

The two different sensors were placed in similar airtight boxes inside the exposure chamber and connected in parallel to the same membrane humidifier to create similar conditions on both the sensors and the tests as explained in section 5.1.2 were performed. The data from the tests were used to compare the two sensors. This setup simulated the conditions of the real experiment but with different flow rates.

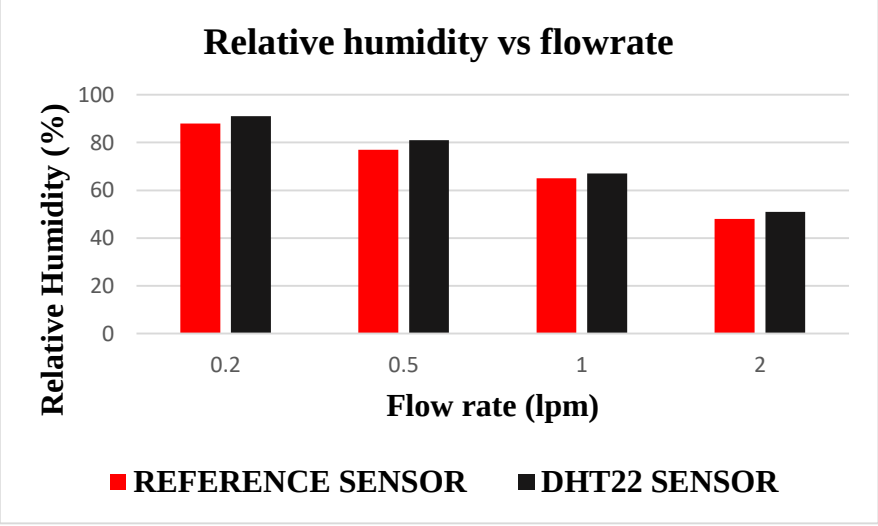

Figure 5.3 Relative humidity as recorded by two different sensors vs flow rates

The results of the sensors at different flow rates were recorded over time. Figure 5.3 shows the average relative humidity at the different flow rates as measured by both the sensors. It can be seen that both the sensors produced very similar results in all cases. This experiment thus verified the capability of the membrane humidifiers and at the same time the reliability of the DHT22 sensor.

5.3 Dilution system effects

There are two dilution systems used in this experiment as explained in previous chapters. The SmartSampler is used as the default dilution system to expose the lung cell models. It operated at a dilution ratio of 10:1. This is the typical dilution ratio that is used in toxicity studies as discussed earlier. The dilution ratio of 5:1 was also explored. A lower dilution ratio meant that there was a higher exhaust flow into the dilution system, which is desirable as a higher dilution ratio meant a higher uncertainty in actual dilution. This is because the dilution air and sampled exhaust are two large regulated flows, which influences the uncertainty in the final dilution ratio. However, running the SmartSampler with a dilution ratio of 5:1 led to water condensation. Thus, it was settled to operate the SmartSampler at 10:1.

The MD-19 rotating disc diluter is the other dilution system used in this experiment. It can operate in a wide range of dilution ratios, ranging from 15:1 to 3000:1. The potentiometer of the MD-19 was set to 20%, which results in a dilution ratio of 75:1. Corrections for the calibration curve of the individual disc used here makes the dilution ratio 78.8:1. Corrections for dilution head temperature make the total dilution ratio 94.5:1. The rounded-off value of 95:1 is used for calculations.

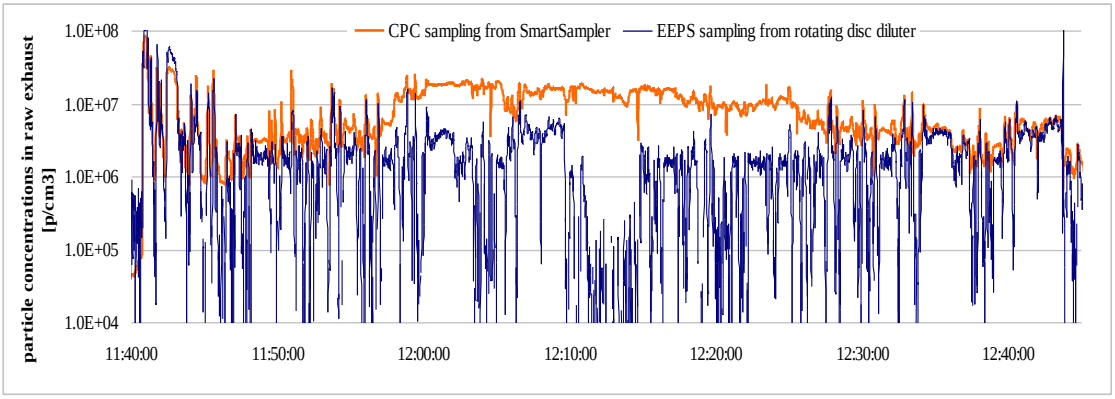

Figure 5.4 Particle concentrations in raw exhaust during two WLTC cycles as measured by EEPS sampling from MD-19 and as measured by CPC sampling from SmartSampler

The results of the calculations performed on two consecutive WLTC cycle runs using the EEPS and CPC are shown in figure 5.4. In these runs, the CPC was sampling from the SmartSampler and the EEPS was sampling from the MD-19. It can be seen that for the most part, the two cycles were comparable. In some parts of the cycle, notably towards the end of the first cycle and the first half of the second cycle, the SmartSampler had more particle concentrations as measured by the CPC. These could be attributed to measurement artefacts or artefacts present in the SmartSampler.

5.3.1 The nucleation hypothesis

To investigate the difference further, the EEPS was used to sample from the SmartSampler for two additional runs, the results of which are shown in terms of a mean size distribution in figure 5.5.

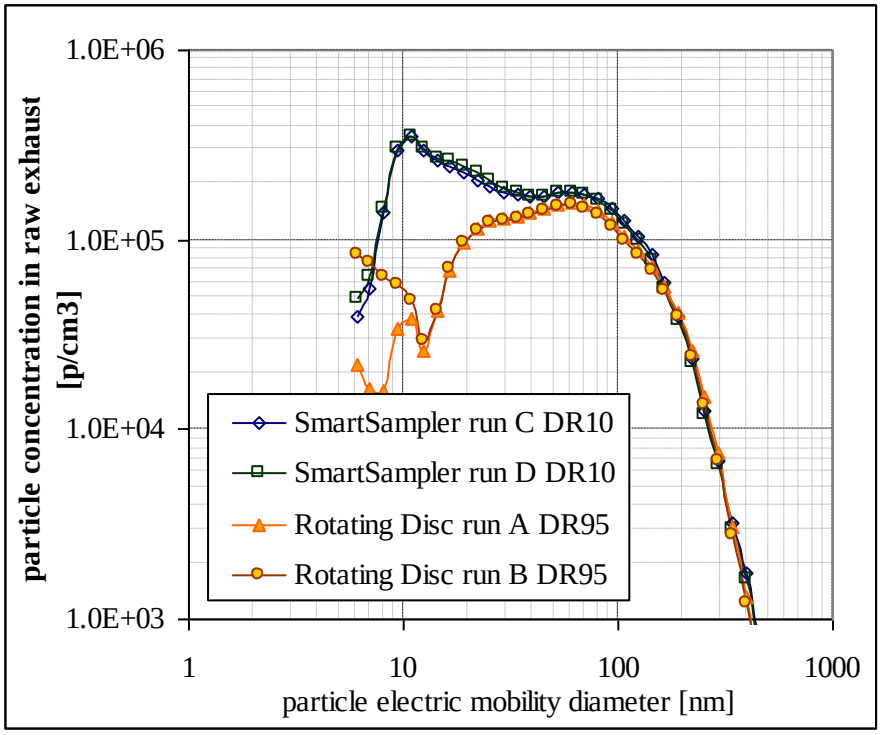

Figure 5.5 Mean particle size distribution over WLTC cycle as measured by EEPS sampling from MD-19 and SmartSampler

It can be seen that there is a strong peak at 10nm for the SmartSampler tests. These peaks are absent in the runs performed with the MD-19. This suggests possible nucleation taking place in the SmartSampler which could be due to the relatively low dilution ratio. This hypothesis is further strengthened by the fact that both the WLTC runs on the SmartSampler had very similar repeatable results. It also shows that both the dilution systems produced a similar result for the particles of higher diameter, over 23nm.

Thus, it can be concluded that the higher particle concentration that is seen at the end of the first WLTC run, at the pause and at the beginning of the second WLTC run is due to the nucleation artefact from the SmartSampler.

During the later stages of testing, a new fuel, E20, containing 20% ethanol by volume was explored. During this change, the SmartSampler's dilution tunnel was taken apart and cleaned on the inside.

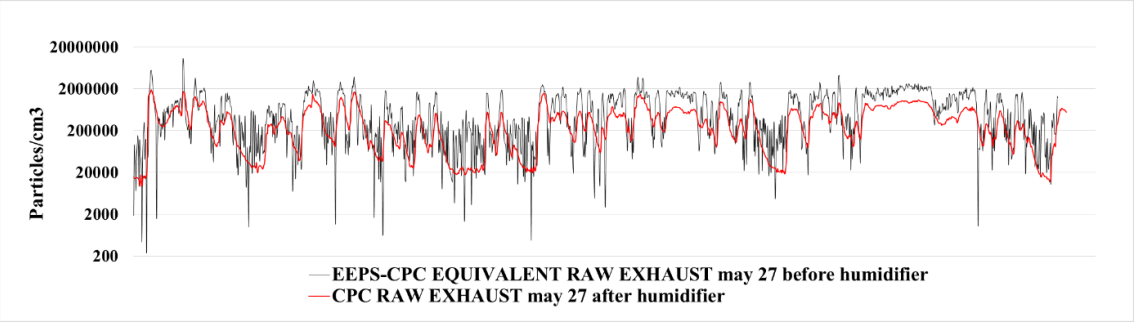

Figure 5.6 WLTC results after cleaning the SmartSampler tunnel

An example of the observations of test runs after the cleaning process is shown in figure 5.6. In this case, the CPC recorded data from the SmartSampler after the humidifier and the EEPS recorded data directly from the MD-19. The observation to note here is the lack of noise on the CPC particle concentrations as opposed to the EEPS recordings that show significant noise.

The CPC data that was analysed before cleaning the SmartSampler contained some noise, though still being lesser than the EEPS. This lack of noise could be attributed to the cleaning of the dilution system, as the EEPS also recorded particle concentrations from the MD-19 during the same cycle.

The extent to which the cleaning affected the nucleation problem could not be exactly measured as the recordings were done by the CPC which does not give size based concentrations as the output. But from the general test results, it could be seen that the particle concentrations from the SmartSampler were not higher than the MD-19 concentrations for the same test cycles, thus making it a possibility that the nucleation problem could have been reduced with cleaning the dilution system.

5.4 Particle losses through the membrane humidifiers

As discussed before, the membrane humidifiers are the only non-conductive components present before the exhaust reaches the exposure boxes where particles are expected to be lost. It is thus imperative to study these losses.

In order to evaluate these particle losses, the mean particle concentrations over a few WLTC cycles were measured at the outlet of the SmartSampler and the MD-19 with both the instruments and the mean particle concentrations at the inlet to the exposure boxes were also measured with both the instruments. The various configurations in which the connections were made as follows:

I. CPC sampling from SmartSampler at the exposure box inlet in the place of the box, EEPS sampling from MD-19.
II. CPC sampling from SmartSampler at the exposure box inlet in parallel with the box, EEPS sampling from MD-19.
III. CPC sampling from MD-19 at the exposure box inlet in the place of the box, EEPS sampling from SmartSampler.
IV. CPC sampling from MD-19 at the exposure box inlet in parallel with the box, EEPS sampling from SmartSampler.

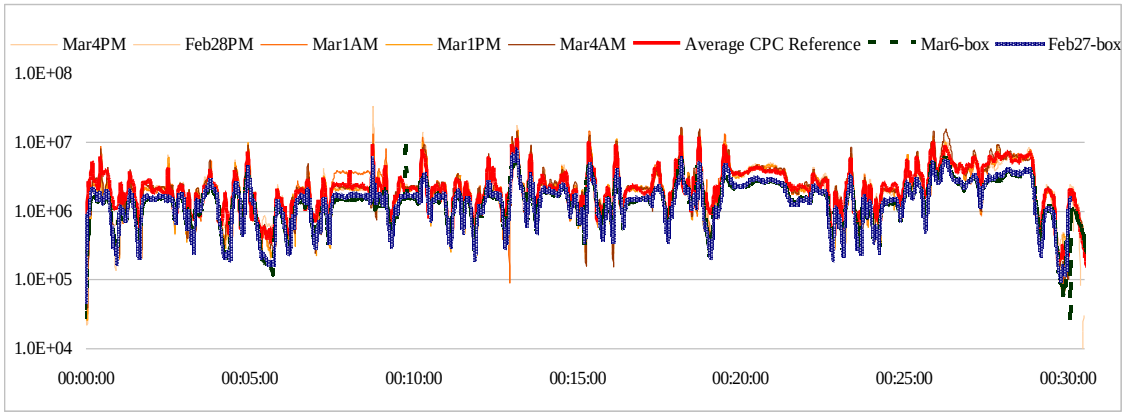

Figure 5.7 Particle concentrations from CPC at exposure box inlet and the SmartSampler outlet (Y-axis units: Particles/cm3)

The mean CPC concentrations measured at the SmartSampler outlet over different cycles are compared with the mean CPC concentrations measured at the exposure box inlet, present after the membrane humidifiers (refer figure 5.7). This specific comparison is done to eliminate any discrepancies caused through instrument variations. The flow at the humidifier is 0.3lpm. The thick red line from figure 5.7 is the average CPC particle concentration per unit time measured over six different warm cycles. The mean particle concentrations were 39.8% lower during the March 6 test and 35.9% lower during the February 27 test than the above mentioned average concentration.

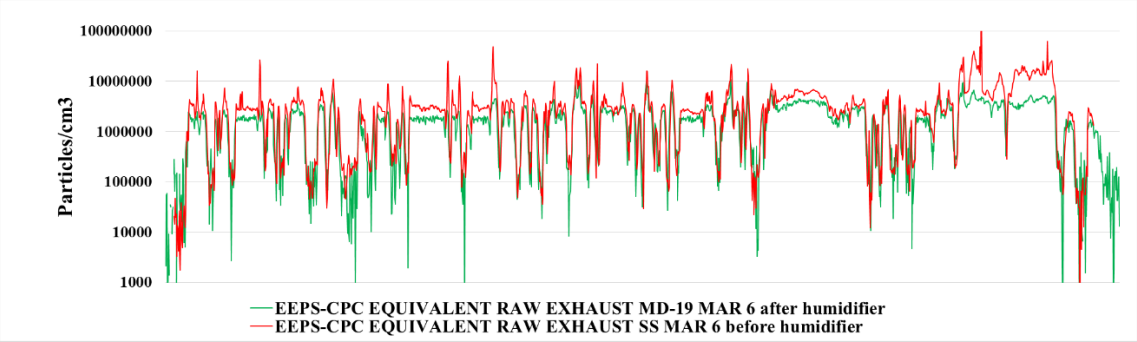

Figure 5.8 Particle concentrations from MD-19 outlet and from SmartSampler measured at exposure box inlet

The mean particle concentrations measured directly from MD-19 by the EEPS and at the inlet of the exposure box from the SmartSampler by the EEPS for consecutive WLTC cycles are compared in figure 5.8. This is done to cross-reference the average particle losses recorded by the CPC with the average particle losses recorded by the EEPS. It should be noted that the MD-19 is also sending particles inside the exposure chamber instead of the SmartSampler in this case.

The particle losses for this particular case were approximately 50%. The higher particle losses, in this case, could be caused due to the higher dilution ratio in the MD-19 as discussed earlier leading to more uncertainties in the actual dilution ratio and also higher uncertainties and artefacts in measurement.

The SmartSampler also had the issue of nucleation leading to a higher particle count, therefore it could have also been one of the reasons for the higher losses as the SmartSampler data is used as a reference in this case. This can be seen in figure 5.8, where the SmartSampler curve has a peak towards the end that is lacking in the MD-19 curve. This further strengthens the nucleation hypothesis as the comparisons done in figure 5.4 were from different WLTC runs, proving that this is a recurring problem.

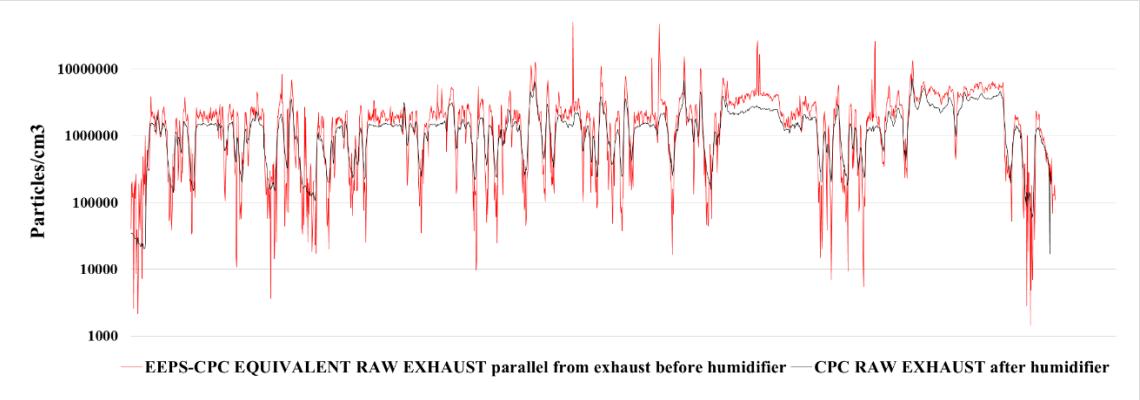

Figure 5.9 Particle concentrations from a parallel connection from the SmartSampler at the exposure box inlet and from MD-19 outlet

The particle concentrations when collected from a line parallel to the exposure box inlet, when compared with the concentrations at the MD-19 outlet during the same WLTC cycle, illustrated in figure 5.9, showed that approximately 33.7% of the particles were lost through the membrane humidifiers. This shows that splitting the sampling line into two thereby increasing the flow through the humidifier to 0.5lpm did not have any considerable effect on the particle losses.

It was proven in earlier sections that 0.5lpm is the maximum flow that could be maintained through the humidifiers. Regular tests conducted with the lung cell samples have a flow of 0.4lpm through them. Figure 5.9 shows that there are no significant changes to particle losses when increasing the flow to 0.5lpm from 0.2lpm in the previous cases.

It can be concluded that about a third of the particles on average were lost within the exposure chamber sampling train. As much of these losses can be attributed to diffusion losses in the humidifiers, a new set of humidifiers that were specifically designed for the use of aerosols was purchased as explained in previous chapters.

The other factors that could influence the particle losses include the distance between the dilution system and the exposure system, the type of pipes used and leakages in the system. These factors were also optimised wherever possible, with more improvements with each iteration.

5.4.1 Particle losses with the new membrane humidifier

As mentioned earlier, a new set of membrane humidifiers were purchased in order to reduce particle losses. These humidifiers were specifically designed for aerosol sampling, contain a single membrane tube, and are made mostly of stainless steel so as to reduce the amount of non-conductive material present in the aerosol path. This could mean both a better performance with exhaust sampling and a lesser performance at humidification. The humidification performance was already tested with the monitoring systems and the results are shown in section 5.1.2. The results of exhaust sampling tests performed with them are discussed in this section.

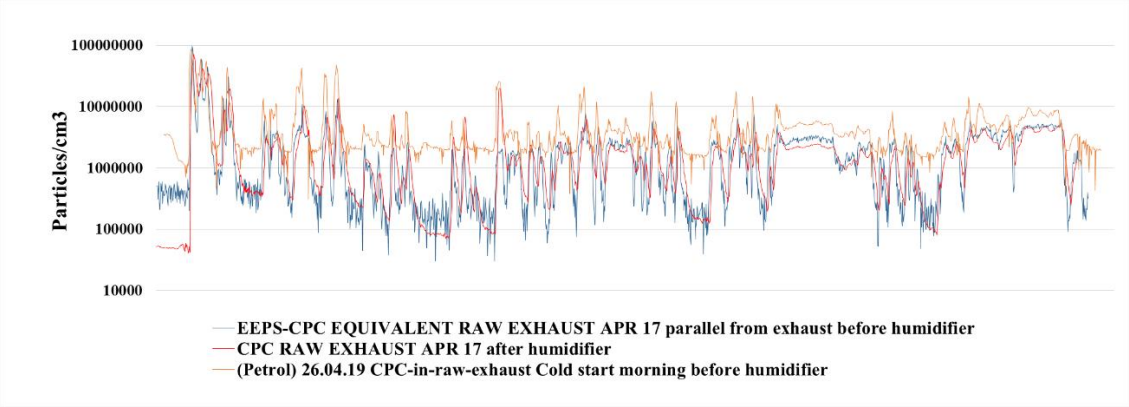

Figure 5.10 Particle concentrations from the SmartSampler at the exposure box inlet, MD-19 outlet and SmartSampler outlet on a different cycle

The particle losses were studied over a WLTC cycle as in the previous cases, as shown in figure 5.10. There was one underlying issue with the analysis of this particular data, as the average particle concentration as measured by the EEPS at the MD-19 outlet is lower than the concentration measured by the CPC at the exposure box inlet, after having passed through the membrane humidifier. It was found to be a singular anomaly, just in this test.

This was a trivial result that could be caused due to multiple reasons, the major one being the uncertainty in the dilution ratio from the MD-19, as discussed earlier. It could also be because of an increase in the artefacts in the SmartSampler. But this was the only set of data available for finding out the particle losses with the new humidifiers with the same fuel. Therefore, a workaround was found.

In order to compare these results, a secondary cold start test data from the SmartSampler measured by the CPC was taken. This was chosen because the particular test in question more closely resembled cold start tests than warm tests. There was still an issue of the cold start test having much more particles than this test too. As a result, the particle losses when compared to the cold start test came out to be approximately around 50%.

This result was initially accepted as it was exactly the same result to the losses obtained during the next test phase with a new fuel. The problem was that though the result was very similar, the cleaning of the SmartSampler could have impacted the results of the next stage of testing. This change thus warranted further investigation into the error with the current data, as it was a change that could have made a difference.

A working compromise was to average out the cold start test data measured from the SmartSampler by the CPC with the initial MD-19 concentrations measured by the EEPS in order to get a closer match to the particle concentrations that could have been recorded from the SmartSampler by the CPC before the humidifier. This method showed that approximately 32% of the particles were lost in the humidifier. This is again around a third of the particles, just as in the case of the old membrane humidifiers. If calculated more accurately, there is around a 5% improvement, as the previous losses were around 36-38%, although it is not a big difference.

This concludes that the humidifiers that were specifically designed for work with aerosols did not have any big impact on the results.

5.4.2 Particle losses with the new fuel

The last stage of testing discussed in this thesis was done with a new ethanol blend gasoline (E20 gasoline) instead of regular E5 gasoline. The factor in study in this thesis, however, is not the new fuel, but the cleaning of the SmartSampler that was performed during the process of changing the system to the new fuel.

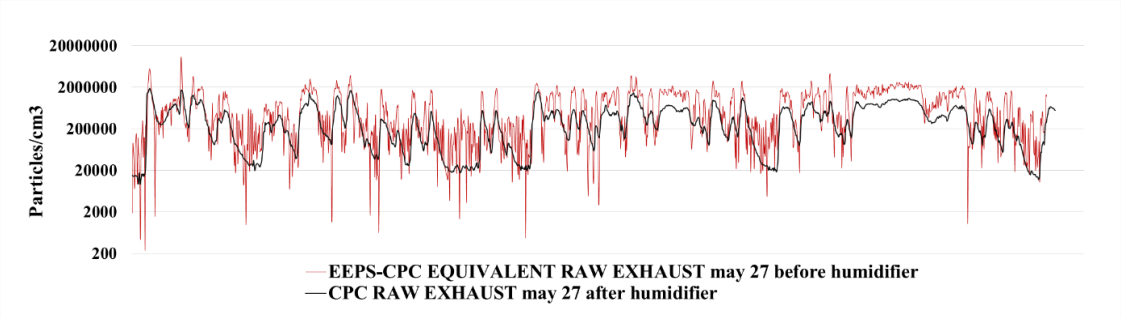

Figure 5.11 Particle concentrations from the SmartSampler at the exposure box inlet and MD-19 outlet

The comparison of particle losses by performing particle concentration measurements before and after the membrane humidifiers (a similar comparison to that shown in figure 5.8) is shown in figure 5.11. The data was not trivial as in the previous scenario where the EEPS recorded lower particle concentrations from the MD-19 than the CPC from the SmartSampler after the membrane humidifier. Since the experimental setup was not changed between the last set of tests and this one, it can be concluded that the trivial nature of the data in the previous case did not have anything to do with the setup.

The comparison in figure 5.11 shows the particle concentrations measured by the EEPS from the MD-19 outlet versus that measured by the CPC from the SmartSampler at the inlet of the exposure box. If there would be no artefacts in the dilution systems, this would suggest that the particle losses between the incubator inlet and the exposure box inlet are 52%. This was very accurate data as the entire dilution system was cleaned prior to the testing procedure. It also hints at another hypothesis that the losses were around 50% throughout the test phases.

6 Discussion and future scope

This chapter deals with general discussions about the project, laying down explanations for some phenomena that were observed. It also deals with suggestions for future developments.

6.1 The dilution systems

The first goal of the thesis was to compare the dilution systems. It could be seen that the dilution systems provided mostly similar results, and the variations could be attributed to the nucleation artefact in the SmartSampler. The SmartSampler was also harder to mount and setup when compared to the MD-19. It also needs an external compressed air supply, which caused problems during some stages of testing due to issues in the air supply. The MD-19 does not have this complication as it does not need any external supply except for the exhaust sample.

Despite this issue, due to the need for a lower dilution ratio, the SmartSampler is the better option to use in the exhaust sampling train. Though a higher dilution ratio in the order of 100:1 provides more realistic exposure conditions, it decreases the dose delivered to the cell models due to practical limits on the length of the exposure. This will make it difficult to study and differentiate the effects of the exhaust from other effects.

The SmartSampler also has a gravimetric sampling system. This allows for further analysis of the particles for comparison with the composition of the exhaust particles versus the reaction of the lung cell culture samples. It is more precise to use the same dilution system for gravimetric sampling and for sampling the cell models as opposed to using the SmartSampler for the gravimetric data and MD-19 for exposing the lung cells, even if the MD-19 could maintain a lower dilution ratio.

Another factor to discuss the general operation of the SmartSampler was the return flow of atmospheric air at 2.0lpm, which was used to compensate the amount of exhaust taken by a parallel line as explained in previous chapters. Each time the gravimetric system was enabled, and the filter sampling was started, the return flow increased by around 0.5 to 1 lpm. This flow decreased by the same amount when the filter sampling was stopped.

This was a consistent observation and could be caused by the sudden opening and closing of the sampling valve. This phenomenon is called ‘water hammer’, which is usually caused during the sudden opening or closing of a valve thereby enabling or limiting sudden flow through a pipe. The sudden opening or closing of valves leads to pressure waves that are caused by this phenomenon, which could lead to vibrations, noise, and also a complete pipe collapse (Lee, et.al, 2010).

It is not cause for huge concern in this setup as the dilution system is designed and manufactured with safety guidelines for the industry. The discussion is focussed rather on the control of the return flow. Each time the gravimetric sampling was started and stopped, the rotameter controlling the return flow had to be adjusted so as to maintain the closed system as originally planned. Manual intervention was thus always necessary to account for the pressure waves. Since it was not a large issue that could be solved in a few seconds before each engine cycle, further steps were not taken to automate the adjustments.

6.2 The connection between losses and artefacts

Particle losses through the sampling system was another topic that was studied in this thesis. The results from the first phase of experimentation showed that one-third of the particles were lost during their journey to the lung cell cultures. However, during the second phase of experimentation with the new membrane humidifiers, the losses seemed to have increased to around 50%. There were two tests, one before the cleaning of the dilution tunnel, and one after.

The result of the first test of about 50% particle losses was initially accepted since it coincided with the result of the second test, as discussed in the previous chapter. A better comparison was then devised with averaging two sets of data, and the resulting losses were 32%. This value fits better with the first phase of experimentation with the old humidifiers.

From the results of the test conducted after cleaning the SmartSampler, it could be seen that the particle losses were 50% when compared with the particle concentrations with the MD-19. This suggests that there could be additional particles coming from the SmartSampler before it was cleaned.

This leads to a new hypothesis that a portion of the particles that were sampled to the lung cell models were in fact artefacts from the SmartSampler. This also effectively explains the nucleation problem, which led to a higher particle concentration in the SmartSampler as opposed to the MD-19 as discussed before. This problem could have thus been solved indirectly through the cleaning procedure.

It also means that the losses in particles through the sampling train could have been higher for the whole experiment. This phenomenon was assessed by making comparisons with the particle concentrations sampled by the CPC at the incubator inlet and at the exposure box inlet. The total losses could be estimated to be around 40%.

Another factor to discuss is the new membrane humidifiers. Although they were specifically designed for work with aerosols, they did not seem to have superior performance to the regular models. Their performance with respect to humidification was however similar to the other set of humidifiers as the flow rate was very low. The difference in performance could perhaps be observed for higher flow rates. This is however not a cause for concern in this project, as the flow rate is limited to only 0.5lpm as is.

6.3 Future scope

The main objective of the phase of the project that has been discussed in the thesis was to design and validate selected components of the exposure chamber and its sampling train. This has been accomplished at a proof of concept level. Following successful validation, some refinements for the components are laid forth in this section.

The major development for the project going forward would be to design and manufacture a more compact exposure chamber for on-road measurements that could maintain the required temperature. The current exposure chamber, though relatively compact, is still larger than it has to be, and uses a lot of space in the engine test cell. A much smaller chamber with a simple temperature control could replace this existing system.

Since it will be designed for this specific application, it could be fitted with special mounts for the exposure boxes, have built-in pipelines, automated flow control and mounts for humidifiers. The built-in pipelines will have an impact on particle losses. Flow control is an important factor as much of the time between consecutive test cycles was spent to verify flows and correct the rotameters. If an automated and specific flow control could be in-built with the chamber, it would save a lot of time and avoid unnecessary accidents and errors in testing. The humidifiers are currently mounted on crudely welded stands, as they were an easy and cost-effective in-house solution for the current setup. The size of the existing exposure chamber also allowed for the stands to be the easiest solution for the current setup, requiring the least amount of modifications to space. This could be also improved with this new smaller chamber.

Multiple personal computers are currently used to record data from and to control the various instruments. This occupies a lot of space in the test cell, which could be solved by installing and calibrating all the software into one single laptop. This change effectively lowers power consumption and saves space.

Industrial mass airflow controllers could be used to replace the existing rotameters. Currently, the rotameters have to be calibrated individually before the start of each test and also constantly monitored to correct flow variations. This problem could potentially be solved with replacing all rotameters with industry-standard digital flowmeters which claim to have more precise performance.

With a higher flow rate of around 2.0lpm through the membrane humidifiers, the particle losses could be further reduced. The problem with this change currently is the reduction in temperature and relative humidity of the sample when coming out of the humidifiers. An additional heat exchanger for the sample could be designed outside the exposure chamber, which would pre-heat the sample to a higher level than the existing heat exchanger in order to achieve high relative humidity before entering the chamber.

All these changes add to the cost and complexity of an already complex system, but over a long period of time, it could prove to be a standard exhaust exposure system for future toxicological studies. The long term goal of the project is the ability to perform on-road tests. The components could be fit into a moving vehicle, with the power consumption in the order of 100W (Vojtisek, et.al, 2019). Portable particle measurement instruments have already been tested extensively in conjunction with rotating disc diluters and less

extensively with proportional gravimetric sampling systems as part of the proposed extension of the EU Real Driving Emissions (RDE) legislation for particle number (Vojtisek, et.al, 2019). The other materials required are small-sized CO_2 tanks and deionized water, which could also be purchased and stored in a moving vehicle quite easily.

The lung cell cultures were also already transported between the toxicological and engine testing laboratories every day throughout the testing period. This amounted to around two and a half hours of transportation in the car every day. They were subject to four WLTC test cycles each day at the engine testing laboratory. The duration of the round trip is equivalent to performing five WLTC test cycles. Thus, in theory, the probability of obtaining similar results when these tests are conducted on a vehicle as it moves around the city is reasonably high.

There is very large uncertainty and complexity in performing these measurements that makes it unideal for type approval legislations, but it could provide very valuable information about the effect of new and emerging engine technology, modifications made on vehicles, new fuels and other changes on human health (Vojtisek, et.al, 2019).

7 Conclusion

A toxicological experiment was set up to study the effects of a Euro 5 Gasoline Direct Injection (GDI) engine on human lung cell tissues. The lung cell cultures used in this experiment were the Human lung cell line BEAS-2B and the 3D lung tissue model MucilAir^{TM} (Epithelix Sarl, Geneva). These cell cultures were exposed over a period of five days, with each day of exposure consisting of four WLTC test runs, two of which were cold start runs and two were warm runs.

The flow of exhaust started at the outlet of the engine exhaust valve and then went through the after-treatment process, after which it was sampled to two dilution systems. Two dilution systems, a gravimetric proportional dilution system – the SmartSampler (AVL) and a rotating disc diluter – the MD-19 (TSI Incorporated) were tested to dilute and sample the exhaust to the exposure system.

The performance of the dilution systems over the course of the test phases was studied in detail. The SmartSampler operated at a low dilution ratio of 10:1. The MD-19 had a disadvantage of not being able to be operated at low dilution ratios, and the effective dilution ratio it operated on was 95:1. The SmartSampler also had the advantage of gravimetric particle sampling for further analysis. The MD-19 was observed to have lesser particle concentrations during the end of a WLTC test cycle and before the beginning of the consecutive WLTC test cycle when compared to the SmartSampler, as the lower dilution ratio and other complex factors led to an issue of nucleation in the latter. The dilution tunnel was eventually cleaned in an attempt to combat some artefacts that could be created inside the tunnel.

After the dilution process, the exhaust flowed inside a toxicological incubator also known as the exposure chamber, which maintained certain conditions for the lung cell models. The conditions required for the survivability of the lung cell cultures were a 5% excess CO_2, an ambient temperature of 37°C, a very high relative humidity of at least 85% and sterile conditions. A CO_2 tank was used to add the required quantity of the gas into the sampling train. Inside the exposure chamber, two membrane humidifiers were used to humidify the sample flow. The sample then flowed into specially designed exposure boxes inside which the lung cell models were present.

A humidity and temperature monitoring system was designed as a part of the thesis work to monitor the relative humidity and temperature of the sample flow in real-time. It was validated by a parallel measurement with a reference sensor.

The entire flow was created via suction pressure from a vacuum pump. Rotameters were used to control the flow rates. The flow at different points was continuously checked and verified via a flow meter. The flow rate at which each lung cell culture sample received the sample was 0.025lpm.

The particle losses in the sampling train were investigated. The highest particle losses, around 40% on average, were observed in the membrane humidifiers. The membrane humidifiers were necessary in order to maintain the high relative humidity required for the experiment. The cleaning process of the SmartSampler helped to reduce some of the artefacts in the sampling system. Categorizing and investigating very small particles is a complicated process, and these were the best conclusions that could be drawn with the existing data.

The preliminary experimental tests that were performed and discussed in this thesis were the first step to designing and developing a robust, easy to set up compact exposure system that could be used to perform toxicological studies during on-road tests, in order to get more realistic data. Although relatively larger partial flow dilution systems were used in this experiment, compact proportional dilution systems are feasible and could be used for the final application.

The complete system that was envisioned in this project could be very useful in future investigations of the effects of new technologies in the field of combustion engines on human health.

The contribution made in this thesis consisted of the following:

1. The design and setting up of the experimental setup including the dilution systems, particle measurement instruments, and the various components inside the exposure chamber excluding the design of the exposure boxes.
2. The humidity and temperature monitoring system with the choice of sensors, machining of the air-tight housing and testing for performance.
3. Finding the flow limitations of the experimental setup with respect to humidity and temperature.
4. Performing toxicity experiments on the apparatus in the engine testing laboratory over the course of the first half of 2019.
5. Analysing data obtained from the particle measurement instruments and investigating the performance of dilution systems and observing the particle losses through the membrane humidifiers.

References

Ankilov, A., Baklanov, A., Colhoun, M., et al. (2002). Particle size-dependent response of aerosol counters. Atmospheric Research, 62(3-4), 209-237

Aosong Electronics Co.,Ltd, Digital-output relative humidity & temperature sensor/module DHT22 (DHT22 also named as AM2302)
https://www.sparkfun.com/datasheets/Sensors/Temperature/DHT22.pdf

Arduino©, 2019. Arduino Mega 2560 REV3.
https://store.arduino.cc/mega-2560-r3

Barter, A, Robert. Toxicity evaluation of Gasoline Exhaust Emissions. Health and Environmental Sciences Department. American Petroleum Institute, Washington, D.C. 20005
https://pdfs.semanticscholar.org/fc60/2633c091b465ef95957adbcdb8c1db3e99fb.pdf

Bischof, Oliver & Krinke, Thomas & Zerrath, Axel & Liu, Wei & Han, Hee-Siew & Hermann, Martyna & Wehner, Birgit & Wiedensohler, Alfred. (2006). Characterization of a Water-based and a new butanol-based Condensation Particle Counter

Centre for Atmospheric Science, 2019, Condensation Particle Counters (CPC)
http://www.cas.manchester.ac.uk/restools/instruments/aerosol/cpc/

Cooney, D. J., & Hickey, A. J. (2011). Cellular response to the deposition of diesel exhaust particle aerosols onto human lung cells grown at the air-liquid interface by inertial impaction. Toxicology in Vitro, 25(8), 1953-1965

DieselNet, 2019, Emission Test Cycles: Worldwide Harmonized Light Vehicles Test Cycle (WLTC)
https://www.dieselnet.com/standards/cycles/wltp.php

DieselNet, 2019. Emission Standards- EU: Cars and Light trucks
https://www.dieselnet.com/standards/eu/ld.php

Elder A., Gelein R., Silva V., Feikert T., et al., Translocation of inhaled manganese oxide particles to the central nervous system, Environ. Health Perspect. 114 (2006) 1172-1178.

European Automobile Manufacturers Association, 2019: Vehicles in Use.
https://www.acea.be/statistics/tag/category/vehicles-in-use

European Environment Agency (EEA): Air quality in Europe – 2018 report. EEA, Copenhagen, 2018.

Geiser M, Lang D. In vitro replica of the inner surface of the lungs for the study of particle-cell interactions. Altex 24, 82-84 (2007)

Geiser, M., Jeannet, N., Fierz, M. and Burtscher, H., 2017. Evaluating adverse effects of inhaled nanoparticles by realistic in vitro technology. Nanomaterials, 7(2), p.49

Health Effect Institute, 2018: State of Global Air. https://www.stateofglobalair.org/sites/default/files/soga-2018-report.pdf

Homolya J., Griffin R.: Sample dilution device-disc diluter. US patent no. 3,803,920; 1972

Hull Rob for thisismoney.uk, 2018. Government's attempts to kill off diesel backfire as official figures show there are MORE on UK roads today than ever before. https://www.thisismoney.co.uk/money/cars/article-5607297/Despite-Governments-best-efforts-diesels-UK-roads-before.html

Ihalainen, M., Jalava, P., Ihantola, T., Kasurinen, S. et al., 2018. Design and validation of an air-liquid interface (ALI) exposure device based on thermophoresis. Aerosol Science and Technology, pp.1-13

International Council on Clean Transportation, 2016. India Bharat Stage VI Emission Standards. https://theicct.org/sites/default/files/publications/India%20BS%20VI%20Policy%20Update%20vF.pdf

Kayes, David & Hochgreb, Simone. (1999). Mechanisms of Particulate Matter Formation in Spark-Ignition Engines. 2. Effect of Fuel, Oil, and Catalyst Parameters. Environmental Science & Technology - ENVIRON SCI TECHNOL. 33. 10.1021/es981100w.

Kooter, I. M., Alblas, M. J., Jedynska, A. D., Steenhof, M. et al., (2013). Alveolar epithelial cells (A549) exposed at the air–liquid interface to diesel exhaust: first study in TNO's powertrain test center. Toxicology in Vitro, 27(8), 2342-2349

Lacroix, G., Koch, W., Ritter, D., Gutleb, A.C. et al., 2018. Air–liquid interface in vitro models for respiratory toxicology research: Consensus workshop and recommendations. Applied in vitro toxicology, 4(2), pp.91-106

Lee, JS., Kim, BK., Lee, WR. et al. J Mech Sci Technol (2010) 24: 1975. https://doi.org/10.1007/s12206-010-0708-6

Majewski, A.W., 2016. Diesel Particulate Matter. https://www.dieselnet.com/tech/dpm.php

Nowak A., Andres H.P.: Measuring Soot Particles from Engines: Recommendations from EMRP-ENV02 Project in WP1. 18th ETH Conference on Combustion Generated Nanoparticles, ETH Zurich, Switzerland, June 22-25, 2014. http://www.nanoparticles.ch/2014_ETH-NPC-18/7-5_Nowak.pdf

Oberdörster G., Sharp Z., Atudorei V., Elder A., et al., Translocation of inhaled ultrafine particles to the brain, Inhal. Toxicol. 16 (2004) 437-445.

Permapure, 2019, FC^{TM} Series Humidifier- User Manual https://www.permapure.com/wp-content/uploads/2016/01/FC-MAN-001-REV-00.pdf

Pham, L., Yang, J., Johnson, K., Durbin, T. et al., 2018. Evaluation of Partial Flow Dilution Systems for Very Low PM Mass Measurements. Emission Control Science and Technology, 4(4), pp.247-259.

Praharaj.K, 2019. Particle emissions from contemporary automobile spark-ignition engines, Master thesis, Faculty of Mechanical Engineering, Czech Technical University, Prague.-Unpublished

Raza, M., Chen, L., Leach, F. and Ding, S., 2018. A review of particulate number (PN) emissions from gasoline direct injection (GDI) engines and their control techniques. Energies, 11(6), p.1417.

Springer G.S. (1973) Particulate Emission from Spark-Ignition Engines. In: Springer G.S., Patterson D.J. (eds) Engine Emissions. Springer, Boston, MA.

Suresh Yuvanesh, 2018. Detection of high particulate matter emitters, Master thesis, Faculty of Mechanical Engineering, Czech Technical University, Prague.

Tippe A, Heinzmann U, Roth C. Deposition of fine and ultrafine aerosol particles during exposure at the air/cell interface. J Aerosol Sci 2002:33;207–218

TSI Incorporated, 2005. Condensation Particle Counter 3022A. https://www.tsi.com/discontinued-products/condensation-particle-counter-3022a-en/

TSI Incorporated, 2005. Model 3090 Engine Exhaust Particle SizerTM Spectrometer. http://www.tsi.com/uploadedFiles/Product_Information/Literature/Spec_Sheets/3090_2980244A.pdf

United States Environmental Protection Agency, 2016. Health and Environmental Effects of Particulate Matter. https://www.epa.gov/pm-pollution/health-and-environmental-effects-particulate-matter-pm

Upadhyay S, Palmberg L, Air-Liquid Interface: Relevant In Vitro Models for Investigating Air Pollutant-Induced Pulmonary Toxicity, Toxicol. Sci. 164 (2018) 21–30. doi:10.1093/toxsci/kfy053.

Vaisala, 2019, HUMICAP® Humidity and Temperature Probe HMP113 https://www.vaisala.com/en/products/instruments-sensors-and-other-measurement-devices/instruments-industrial-measurements/hmp113

Vojtisek, M., Rameswaran, R., Praharaj, K., et.al, Assessing exhaust toxicity with biological detector: Configuration of portable air-liquid interface human lung cell model exposure system, sampling train and test conditions. SAE- 19ICENA-0314/2019-24-0050 – Unpublished

Witze, P. O.; Green, R. M. SAE Tech. Pap. Ser. 1997, No. 970866.

List of figures

Figure 1.1 Size distribution of particulate matter (Majewski, 2016) 8
Figure 1.2 Number-weighted mean and mode particle sizes vs. equivalence ratio for two vehicles (Kayes, et.al, 1999) 9
Figure 1.3 PM_{10} concentrations in 2016 with respect to daily limit value (EEA, Air quality in Europe, 2018a) 12
Figure 3.1 WLTC cycle for Class 3b vehicles (Dieselnet, 2019) 18
Figure 4.1 Exposure system sampling train (Vojtisek, et.al, 2019) 20
Figure 4.2 Experimental setup 21
Figure 4.3 AVL SmartSampler 22
Figure 4.4 Exhaust dilution system (Vojtisek, et.al, 2019) 23
Figure 4.5 MD-19 Rotating disc diluter 23
Figure 4.6 The inside of the exposure chamber 24
Figure 4.7 Principle of FC™ Series Humidifiers (PermaPure, 2019) 25
Figure 4.8 Exposure box with a sample divider head showing paths for flow division (Vojtisek, et.al, 2019) 26
Figure 4.9 CFD Flow analysis to optimise gap between distributor head and lung cell inserts 27
Figure 4.10 DHT22 temperature and humidity sensor (Aosong Electronics Co.,Ltd, 2019) 28
Figure 4.11 Humidity and Temperature box 29
Figure 4.12 Engine Exhaust Particle Sizer flow schematic (TSI Incorporated, 2005) ... 30
Figure 4.13 Schematic of a Condensation Particle Counter (Centre for Atmospheric Science, 2019) 32
Figure 4.14 Schematic of flow rates 33
Figure 4.15 Comparison of the response characteristics of the TSI 3022A CPC with respect to NaCl, Ag and Tungsten oxide test aerosols (Ankilov, 2002) 35
Figure 5.1 Relative humidity vs time with different flow rates 39
Figure 5.2 Temperature vs time for different flow rates 39
Figure 5.3 Relative humidity as recorded by two different sensors vs flow rates 40
Figure 5.4 Particle concentrations in raw exhaust during two WLTC cycles as measured by EEPS sampling from MD-19 and as measured by CPC sampling from SmartSampler 41

Figure 5.5 Mean particle size distribution over WLTC cycle as measured by EEPS sampling from MD-19 and SmartSampler..... 42
Figure 5.6 WLTC results after cleaning the SmartSampler tunnel..... 43
Figure 5.7 Particle concentrations from CPC at exposure box inlet and the SmartSampler outlet (Y-axis units: Particles/cm3) 44
Figure 5.8 Particle concentrations from MD-19 outlet and from SmartSampler measured at exposure box inlet..... 45
Figure 5.9 Particle concentrations from a parallel connection from the SmartSampler at the exposure box inlet and from MD-19 outlet..... 46
Figure 5.10 Particle concentrations from the SmartSampler at the exposure box inlet, MD-19 outlet and SmartSampler outlet on a different cycle..... 47
Figure 5.11 Particle concentrations from the SmartSampler at the exposure box inlet and MD-19 outlet..... 49

List of tables

Table 1.1 Air quality standards for the protection of health for PM, given in the EU Ambient Air Quality Directives (EEA, Air quality in Europe, 2018) 11
Table 4.1 Specifications of DHT22 sensor (Aosong Electronics Co.,Ltd, 2019)..... 28

Appendix

A. Technical data of Engine Exhaust Particle Sizer

Specifications	**Range**
Particle size range	5.6 to 560 nm
Particle size resolution	16 channels per decade (32 total)
Charger mode of operation	Unipolar diffusion charger
Time resolution	10 size distributions/sec
Flow rates Sample flow	10 l/min
Sheath air	40 l/min
Inlet sample temperature	10 to 52°C
Operating temperature	0 to 40°C
Storage temperature	-20 to 50°C
Atmospheric pressure correction range	70 to 103 kPa (700 to 1034 mbar)
Humidity	0 to 90% RH (noncondensing)
User interface	Rotary knob and display; EEPS software
Computer requirements	Pentium® 4 processor, 2 GHz speed or better, at least 512 MB RAM
Operating system required	Windows® XP or better
Weight	32 kg
Sample inlet	3/8-in. Outer diameter (without inlet cyclone)
Cyclone inlet	3/8-in. Outer diameter
Exhaust/Outlet	3/8-in. Outer diameter
Power requirements	100 to 240 VAC, 50/60 Hz, 250W

Technical data of Engine Exhaust Particle Sizer (TSI Incorporated, 2005)

B. Technical data of Condensation Particle Counter

Specifications	**Range**
Particle size range	Minimum detectable particle: 50% of 7-nm particles Maximum detectable particle: >3 µm
Particle concentration range	0 to 9.99 × 106 particles/cm3; counts single particles in concentrations from 0 to 104 particles/cm3, photometric calibration from 104 to 107 particles/cm3; provides running-average over 1, 2, 20, and 200 seconds depending on concentration range; display updated every second
Concentration accuracy	±10% up to 5 × 105 particles/cm3, ± 20% from 5 × 105 to 107 particles/cm3; coincidence less than 2% at 104 particles/cm3; live-time particle counting from 103 to 104 particles/cm3 provides automatic correction for coincidence
False background counts	<0.01 particle/cm3
Response time	<13 sec for 95% response to concentration step change when sampling in high-flow mode; <20 sec for low-flow mode
Aerosol medium	Recommended for use with air; safe for use with

	Inert gases such as nitrogen, argon, and helium (Performance specifications are for air.)
Signal-to-noise ratio	25:1 nominal
Light source	Stable, 5-mW, 780-nm laser diode
Flow	Aerosol flow rate: 300 ± 15 cm3/min High-flow inlet: 1500 ± 150 cm3/min Low-flow inlet: 300 ± 15 cm3/min
Condensing liquid	Working fluid: Reagent-grade n-butyl alcohol (not included) Filling system: Electronic liquid-level sensor initiates automatic filling as needed, requires connection to fill bottle (provided with instrument
Operating temperatures	Saturator: 35 ± 0.3 °C Condenser: 10 ± 0.3 °C Optics: 36 ± 2.0 °C
Communications	Protocol: Command set based on ASCII characters Interface: RS-232, 9-pin, “D” subminiature connector, pinouts compatible with standard IBM-style serial cables and interfaces
Outputs	Digital display: Concentration, total counts, status (temperatures, aerosol flow, photodetector voltage) Analog: BNC connection, 0 to 10 volts, user-selectable function

	output (linearized concentration, log concentration, aerosol flow, pump control, photodetector voltage) (For use in TSI SMPS systems, a Host mode allows output to 11 volts.) Pulse: BNC connection, 13V square pulse, typically 3.3 µsec wide
Software	Supplied with CPCount™ Software
Calibration	Recommended annually; calibrated with 50-nm monodisperse NaCl using primary differential mobility analyzer method
Power requirements	100/120/230/240 VAC, 50/60 Hz, 200 W maximum
Dimensions (LWH)	24 cm × 38 cm × 20 cm (9.5 in. × 15 in. × 8 in.), not including fill bottle and bracket
Weight	: 12.5 kg
Environmental operating conditions	Ambient temperature range: 10 to 35 °C Ambient humidity range: 0 to 90% RH, noncondensing

Technical data of Condensation Particle Counter (TSI Incorporated, 2019)

C. Specifications of Arduino Mega 2560 REV3

Specifications	**Range**
Microcontroller	ATmega2560
Operating Voltage	5V
Input Voltage (recommended)	7-12V
Input Voltage (limit)	6-20V
Digital I/O Pins	54 (of which 15 provide PWM output)
Analog Input Pins	16
DC Current per I/O Pin	20 mA
DC Current for 3.3V Pin	50 mA
Flash Memory	256 KB of which 8 KB used by bootloader
SRAM	8 KB
EEPROM	4 KB
Clock Speed	16 MHz
LED_BUILTIN	13
Length	101.52 mm
Weight	37 g
Width	53.3 mm

Technical data of Arduino Mega 2560 REV3 (Arduino, 2019)

D. Arduino program

```
#include <DHT.h>

#define DHT1TYPE DHT22 // DHT 22
#define DHT2TYPE DHT22 // DHT 22
#define DHT1PIN 7
#define DHT2PIN 8
DHT dht1(DHT1PIN, DHT1TYPE);
DHT dht2(DHT2PIN, DHT2TYPE);
void setup(){
  Serial.begin(9600);
    dht1.begin();
  dht2.begin();
}

void loop()
{
//  int chk = dht1.read11(DHT1PIN);
 // int chk2 = dht2.read11(DHT2PIN);
   float h1 = dht1.readHumidity();
  float t1 = dht1.readTemperature();
  float h2 = dht2.readHumidity();
  float t2 = dht2.readTemperature();
  Serial.print("#S|DATAREAD|[");
  Serial.print("      ");
  Serial.print(t1);
  Serial.print(";");
  Serial.print("       ");
  Serial.print(h1);
```

```
Serial.println(     "]#");
Serial.print("#S|DATAREAD2|[");
Serial.print("      ");
Serial.print(t2);
Serial.print(";");
Serial.print("       ");
Serial.print(h2);
Serial.println(     "]#");

delay(1000);

}
```